Contribution from the Central Research and Development Department, Experimental Station 328, E. I. du Pont de Nemours & Company, Wilmington, Delaware 19898

Electrocrystallization and Structural and Physical Properties of Charge-Transfer Complexes Derived from $[(\eta^6\text{-}C_6Me_6)_2M]^{2+}$ (M = Fe, Ru) and TCNQ (TCNQ = Tetracyanoquinodimethane)

M. D. Ward* and D. C. Johnson†

Received May 28, 1987

Charge-transfer complexes $[(\eta^6\text{-}C_6Me_6)_2M][TCNQ]_x$ (M = Fe, Ru; x = 2, 4; TCNQ = tetracyanoquinodimethane) and $[(\eta^6\text{-}C_6Me_6)_2M][TCNQ']_2$ (M = Fe, Ru; TCNQ′ = $(TCNQ)Cl_2$, $(TCNQ)F_4$) are prepared with electrocrystallization techniques by reduction of TCNQ or TCNQ′ in the presence of $[(\eta^6\text{-}C_6Me_6)_2M]^{2+}$. Selectivity toward the TCNQ phases can be directed electrochemically by control of the electrode potential during electrocrystallization. At very negative potentials a poorly conducting 1:2 phase is formed as a deep purple crystalline solid, whereas more positive potentials favor a black, conducting 1:4 phase. The selectivity is determined by the potential-dependent concentrations of TCNQ and $TCNQ^-$ at the electrode. Complexes with anions possessing halogen substituents (e.g., $(TCNQ)Cl_2$, $(TCNQ)F_4$) only crystallize as 1:2 phases, presumably due to decreased Coulombic repulsion between associated anions. Conversely, only conducting phases are observed with derivatives possessing electron-donating substituents (e.g., $(TCNQ)Me_2$, $TCNQ(OMe)_2$). The single-crystal X-ray structures of the 1:2 phases, which all crystallize in the triclinic $P\bar{1}$ space group, are reported. For $[(\eta^6\text{-}C_6Me_6)_2M][TCNQ]_2$, for M = Fe [Ru], a = 10.167 (2) [11.350 (7)] Å, b = 11.281 (3) [9.163 (3)] Å, c = 9.187 (1) [10.184 (5)] Å, α = 111.08 (2) [91.82 (5)]°, β = 98.10 (1) [110.89 (4)]°, γ = 92.37 (2) [98.19 (3)]°, V = 968.5 [976 (2)] Å^3, Z = 1 [1], d = 1.35 [1.42] g cm^{-3}, R_u = 0.046 [0.039], and R_w = 0.052 [0.043]. For $[(\eta^6\text{-}C_6Me_6)_2M][(TCNQ)F_4]_2$, for M = Fe [Ru], a = 10.140 (3) [10.143 (8)] Å, b = 10.907 (4) [10.830 (2)] Å, c = 10.056 (4) [10.092 (5)] Å, α = 95.74 (3) [92.11 (4)]°, β = 93.72 (3) [96.40 (3)]°, γ = 92.35 (3) [94.40 (5)]°, V = 1103.0 [1097 (2)] Å^3, Z = 1 [1], d = 1.50 [1.57] g cm^{-3}, R_u = 0.068 [0.065], and R_w = 0.082 [0.073]. For $[(\eta^6\text{-}C_6Me_6)_2M][(TCNQ)Cl_2]_2$, for M = Fe [Ru], a = 9.985 (6) [9.993 (11)] Å, b = 11.116 (5) [11.225 (10)] Å, c = 9.725 (7) [9.838 (6)] Å, α = 104.28 (7) [89.21 (8)]°, β = 98.07 (5) [75.36 (7)]°, γ = 89.88 (6) [81.98 (7)]°, V = 1035 (2) [1057 (2)] Å^3, Z = 1 [1], d = 1.49 [1.42] g cm^{-3}, R_u = 0.078 [0.069], and R_w = 0.097 [0.075]. The structures of the $[(\eta^6\text{-}C_6Me_6)_2M]^{2+}$ cations are reported here for the first time; the average Fe–C, C–C, and C–Me distances are 2.156, 1.411, and 1.505 Å, respectively, whereas the average Ru–C, C–C, and C–Me distances are 2.257, 1.426, and 1.501 Å, respectively. The 1:2 phases possess dimer dianions that exhibit ring–ring overlap and intradimer separations (Å) decreasing in the order TCNQ (3.23) > $(TCNQ)Cl_2$ (3.21) > $(TCNQ)F_4$ (3.17). The $[TCNQ]_2^{2-}$ dimer forms mixed-stack linear chains with the organometallic dications, i.e., ...DAADAADAA..., with the molecular planes of the $[TCNQ]_2^{2-}$ dimer parallel to the hexamethylbenzene rings of the cations. The interplanar separations between the hexamethylbenzene ligand and the nearest TCNQ anion are greater than 3.6 Å. Extended mixed-stack linear chains are also observed when TCNQ′ = $(TCNQ)Cl_2$ or $(TCNQ)F_4$; however, the $[TCNQ']_2^{2-}$ dimer is stacked "end on" between the cations with the long molecular axes of the TCNQ anions roughly parallel to the linear-chain axes. Close intermolecular contacts between the cyano nitrogen atoms and the ring carbons of the cation that are significantly less than the sum of the van der Waals radii are observed, suggesting a unique type of donor–acceptor interaction. The compounds with 1:2 stoichiometry have relatively low conductivities ($\sigma_{300\,K} < 10^{-7}\ \Omega^{-1}\ cm^{-1}$) and diamagnetic, temperature-independent magnetic susceptibilities. In contrast, the 1:4 phases exhibit much higher conductivity ($\sigma_{300\,K} = 0.1\ \Omega^{-1}\ cm^{-1}$) with temperature dependence indicating semiconducting behavior (E_A = 0.06 eV), which is explained in terms of electron localization along extended TCNQ arrays as a result of Coulombic repulsion. The 1:4 phases exhibit temperature-dependent paramagnetic susceptibilities consistent with the random exchange Heisenberg antiferromagnetic exchange (REHAC) model.

Introduction

The design of new low-dimensional solids[1] with desirable properties requires adequate understanding of the factors that affect the formation of different structural phases and elucidation of the structure–function relationships in these materials. We have been particularly interested in charge-transfer solids possessing organometallic components since generally the physical and chemical characteristics of this class of reagents are readily modified. The diverse variety of these reagents promises to facilitate systematic investigation of factors that influence the structure and properties of low-dimensional solids. To date, well-characterized examples of charge-transfer complexes incorporating organometallic donors are rather limited in number compared to materials with exclusively organic components. Most notable among these have been the decamethylferrocenium–TCNQ complexes reported to form three different phases: paramagnetic $[(\eta^5\text{-}C_5Me_5)_2Fe]_2[TCNQ]_2$,[2] metamagnetic $[(\eta^5\text{-}C_5Me_5)_2Fe][TCNQ]$,[3] and conductive $[(\eta^5\text{-}C_5Me_5)_2Fe][TCNQ]_2$.[4] Bis(toluene)chromium has also been reported to form $[(\eta^6\text{-}C_6H_5CH_3)_2Cr][TCNQ]$ and $[(\eta^6\text{-}C_6H_5CH_3)_2Cr][TCNQ]_2$;[5,6] the latter was reported to exhibit significant conductivity. Recently, the conducting phases $[(\eta^5\text{-}C_5H_5)Fe(\eta^6\text{-}C_6H_3Me_3)][TCNQ]$ and $[(\eta^5\text{-}C_5H_5)Fe(\eta^6\text{-}C_6Me_6)][TCNQ]$ were also reported.[7] Common traits among these complexes are the unipositive charge and planar aromatic ligands in the organometallic component, which probably facilitates molecular packing. In an effort to further understand the role of organometallic constituents in charge-transfer complexes, we have been investigating charge-transfer solids with $[(\eta^6\text{-arene})_2M]^{2+}$ (M = Fe, Ru) cations.[8] Although these cations have been extensively investigated with regard to their physical[9] and electronic[10] properties, their role as components in charge-

* To whom correspondence should be addressed.
† Present address: Department of Chemistry, University of Oregon, Eugene, OR 97403.

(1) *Extended Linear Chain Compounds*; Miller, J. S., Ed.; Plenum: New York, 1981–1983; Vol. 1–3.
(2) (a) Reis, A. H., Jr.; Preston, L. D.; Williams, J. M.; Peterson, S. W.; Candela, G. A.; Swartzendruber, L. J.; Miller, J. S. *J. Am. Chem. Soc.* **1979**, *101*, 2756. (b) Miller, J. S.; Reis, A. H., Jr.; Candela, G. A. *Lect. Notes Phys.* **1978**, *96*, 313.
(3) Miller, J. S.; Reis, A. H., Jr.; Gebert, E.; Ritsko, J. J.; Salaneck, W. R.; Kovnat, L.; Cape, T. W.; Van Duyne, R. P. *J. Am. Chem. Soc.* **1979**, *101*, 7112.
(4) Ritsko, J. J.; Nielsen, P.; Miller, J. S. *J. Chem. Phys.* **1977**, *67*, 687.
(5) Shibaeva, R. P.; Atovmyan, L. O.; Rozenberg, L. P. *J. Chem. Soc. D* **1969**, 649.
(6) Shibaeva, R. P.; Atovmyan, L. O.; Orfanova, M. N. *J. Chem. Soc. D* **1969**, 1494.
(7) Lequan, R.-M.; Lequan, M.; Jaouen, G.; Ouahab, L.; Batail, P.; Padiou, J.; Sutherland, R. G. *J. Chem. Soc., Chem. Commun.* **1985**, 116.
(8) (a) Helling, J. F.; Braitsch, D. M. *J. Am. Chem. Soc.* **1970**, *92*, 7207. (b) Bennett, M. A.; Matheson, T. W. *J. Orgnomet. Chem.* **1979**, *175*, 87.
(9) (a) Michaud, P.; Mariot, J.-P.; Varret, F.; Astruc, D. *J. Chem. Soc., Chem. Commun.* **1982**, 1383. (b) Finke, R. G.; Voegeli, R. H.; Laganis, E. D.; Boekelheide, V. *Organometallics* **1983**, *2*, 34. (c) Laganis, E. D.; Voegeli, R. H.; Swann, R. T.; Finke, R. G.; Hopf, H.; Boekelheide, V. *Organometallics* **1982**, *1*, 11.

0020-1669/87/1326-4213$01.50/0 © 1987 American Chemical Society

transfer complexes has not been thoroughly explored. Our recent observation[11] that the mixed-stack linear-chain complexes $[(\eta^6\text{-}C_6Me_3H_3)_2M][C_6(CN)_6]$ (M = Fe, Ru) exhibit significant donor–acceptor interactions as a result of close face-to-face approach of the polycyano anion and the arene ligands indicated that these species were promising candidates for new low-dimensional materials. These charge-transfer solids exhibited structural characteristics reminiscent of organic DA solids,[12] although their electronic properties (i.e. charge-transfer transition energies) were significantly affected by the identity of the metal atom.

In addition, we have also been investigating the role of electrochemical parameters in electrocrystallization of charge-transfer complexes. Our earlier observations[13] of potential- and current-dependent phase selectivity in the synthesis of decamethylferrocenium–TCNQ complexes suggested that this was a convenient technique for the selective growth of different phases of low-dimensional solids, including poorly conducting charge-transfer complexes. We describe herein the electrochemical synthesis and structural and physical properties of the charge-transfer complexes $[(\eta^6\text{-}C_6Me_6)_2M][TCNQ]_x$ (M = Fe, Ru; x = 2, 4) and $[(\eta^6\text{-}C_6Me_6)_2M][TCNQ']_2$ (M = Fe, Ru; TCNQ′ = $(TCNQ)Cl_2$, $(TCNQ)F_4$).

Results

Electrochemical Synthesis. Charge-transfer complexes are commonly prepared by in situ electron transfer between donors and acceptors. The redox potentials reported for $[(\eta^6\text{-}C_6Me_6)_2M]^{2+}/[(\eta^6\text{-}C_6Me_6)_2M]^+$ (M = Fe, E° = −0.24 V vs SCE; M = Ru, E° = −1.01 V[9b]) indicated that reduction of TCNQ by the monocations was thermodynamically favorable ($E^\circ_{TCNQ/TCNQ^-}$ = +0.19 V). However, metathesis routes, either conventional or electrochemical, were preferred for the synthesis of the charge-transfer complexes described below owing to the instability of $[(\eta^6\text{-}C_6Me_6)_2M]^+$ in solvents compatible with the solubility of TCNQ.

When 2 equiv of $[Bu_4N][TCNQ]$ was added to a solution containing 1 equiv of $[(\eta^6\text{-}C_6Me_6)_2M][X]_2$ (M = Fe, Ru), dark purple microcrystalline $(\eta^6\text{-}C_6Me_6)_2M][TCNQ]_2$ (**1**) precipitated immediately, leaving a nearly colorless solution (eq 1). Single

$$[(\eta^6\text{-}C_6Me_6)_2M][X]_2 + 2[Bu_4N][TCNQ] \rightarrow \begin{array}{l} M = Fe,\ X = PF_6 \\ M = Ru,\ X = BF_4 \end{array} \quad \begin{array}{c} [(\eta^6\text{-}C_6Me_6)_2M][TCNQ]_2 \\ \mathbf{1a},\ M = Fe \\ \mathbf{1b},\ M = Ru \end{array} \quad (1)$$

crystals for X-ray analysis could not be obtained by conventional recrystallization methods due to the negligible solubility of **1**. Therefore, slow-diffusion methods were used, affording deep purple, nonconducting crystals of **1**.

The infrared spectrum of **1a** and **1b** exhibited an intense ν_{CN} band at 2180 cm^{-1}, consistent with the presence of a singly reduced TCNQ species. This asymmetric ν_{CN} stretch is sensitive to the extent of reduction of TCNQ species[14] (2220 cm^{-1} for TCNQ to 2180 cm^{-1} for isolated $TCNQ^-$) due to population of the out-of-plane antibonding π b_{3g} orbital,[15] which results in a decrease in bond order between carbon and nitrogen.

Although electrocrystallization is a preparative method generally reserved for highly conducting linear-chain compounds, we have recently reported that poorly conducting decamethylferrocenium–TCNQ charge-transfer complexes can be conveniently prepared by electrochemical techniques.[13] Electrocrystallization is essentially a controlled metathesis technique wherein the introduction rate of either the donor or acceptor species can be precisely controlled by the applied current or potential. Provided the desired product is insoluble and one of the reagents is electrochemically inactive under the electrolysis conditions, crystal growth at the working electrode can be accomplished. Since the potential for reduction of the metallocenes $[(\eta^6\text{-}C_6Me_6)_2M]^{2+}$ is far negative of the TCNQ reduction potential, the latter can be selectively reduced in the presence of the dications. Indeed, when reduction of TCNQ was performed in acetonitrile or nitromethane at platinum electrodes in the presence of $[(\eta^6\text{-}C_6Me_6)_2M]^{2+}$ at −0.1 V, crystal growth was observed instantaneously at the electrode surface (eq 2). Under these conditions the 1:2 phases

$$2TCNQ + 2e^- \xrightarrow[E_{app} = -0.1\ V]{[(\eta^6\text{-}C_6Me_6)_2M]^{2+}} \begin{array}{c} [(\eta^6\text{-}C_6Me_6)_2M][TCNQ]_2 \\ \mathbf{1a},\ M = Fe \\ \mathbf{1b},\ M = Ru \end{array} \quad (2)$$

$$4TCNQ + 2e^- \xrightarrow[E_{app} = +0.3\ V]{[(\eta^6\text{-}C_6Me_6)_2M]^{2+}} \begin{array}{c} [(\eta^6\text{-}C_6Me_6)_2M][TCNQ]_4\cdot xS \\ \mathbf{2a},\ M = Fe \\ \mathbf{2b},\ M = Ru \\ S = CH_3CN,\ CH_3NO_2 \end{array} \quad (3)$$

1a,b were produced in nearly quantitative yields, corroborated by the high Faradaic yields (95% based on **1a,b**). However, very small amounts of a black, conductive crystalline solid were occasionally observed under these conditions when M = Fe. Application of more positive potentials during the synthesis resulted in greater amounts of the black phase in both cases. This phase exhibited a room-temperature conductivity $\sigma_{300\,K}$ = 0.1 Ω^{-1} cm^{-1} (vide infra) and was exclusively formed at +0.3 V for both the iron and ruthenium derivatives.

Elemental analysis and Faradaic yields indicated that the black phase was the 1:4 phase **2a,b** (eq 3). Analyses also confirmed the presence of two solvent molecules when S = nitromethane, whereas acetonitrile was readily lost from the compound. Crystals of the conducting phase possessed an unusual "helical" morphology, giving the appearance of continuous wires. Conductivity measurements indicated reasonable conductivity along the length of these crystals (ca. 0.01 Ω^{-1} cm^{-1}), consistent with the presence of continuous conductive paths. The infrared spectra of **2** exhibited ν_{CN} absorptions at 2200 cm^{-1}, suggesting partial TCNQ reduction. If a linear dependence of the ν_{CN} frequencies on the extent of reduction is assumed,[16,17] these data are consistent with the presence of $TCNQ^{0.5-}$.

The relative amounts of **1** and **2** in the product varied systematically at intermediate potentials, with the 1:2 phase favored at more negative potentials. This is readily observed by visual examination and by the relative intensities of the ν_{CN} absorptions for mixtures of **1** and **2** produced at different potentials, as well as by powder X-ray diffraction studies. The high selectivity toward **1** at −0.1 V was observed even when electrolyses were terminated when the number of TCNQ equivalents consumed reached only 10% of the initial concentration. Since the bulk solution contains a large excess of TCNQ at the end of the electrolysis under these conditions, this rules out the possibility that **1** is readily converted to **2** during or after crystallization. That is, the stoichiometry of the electrochemically grown phases does not simply reflect the concentrations of TCNQ and $TCNQ^-$ in solution near the end of the electrolyses; presumably their negligible solubilities mitigate

(10) (a) Anderson, S. E., Jr.; Drago, R. S. *Inorg. Chem.* **1972**, *11*, 1564. (b) Clack, D. W.; Warren, K. D. *J. Organomet. Chem.* **1978**, *152*, C60. (c) Brintzinger, H.; Palmer, G.; Sands, R. H. *J. Am. Chem. Soc.* **1965**, *87*, 623. (d) Morrison, W. H.; Ho, E. Y.; Hendrickson, D. N. *Inorg. Chem.* **1975**, *14*, 500. (e) Anderson, S. E., Jr.; Drago, R. S. *J. Am. Chem. Soc.* **1970**, *92*, 4244.
(11) Ward, M. D. *Organometallics* **1986**, *6*, 754.
(12) Herbstein, F. H. *Perspectives in Structural Chemistry*; Dunitz, J. D., Ibers, J. A., Eds.; Wiley: New York, 1971; Vol. IV, p 166.
(13) Ward, M. D. *Inorg. Chem.* **1986**, *25*, 4444.
(14) Bozio, R.; Zanon, I.; Girlando, A.; Pecile, C. *J. Chem. Soc., Faraday Trans. 2* **1978**, *74*, 235.
(15) Miller, J. S.; Zhang, J. H.; Reiff, W. M.; Dixon, D. A.; Preston, L. D.; Reis, A. H., Jr.; Gebert, E.; Extine, M.; Troup, J.; Epstein, A. J.; Ward, M. D. *J. Phys. Chem.* **1987**, *91*, 4344.
(16) (a) Chappell, J. S.; Bloch, A. N.; Bryden, W. A.; Maxfield, M.; Poehler, T. O.; Cowan, D. O. *J. Am. Chem. Soc.* **1981**, *103*, 2442. (b) Van Duyne, R. P.; Cape, T. W.; Suchanski, M. R.; Siedle, A. R. *J. Phys. Chem.* **1986**, *90*, 739.
(17) (a) Friedrich, H. B.; Person, W. B. *J. Chem. Phys.* **1966**, *44*, 2161. (b) Jurgensen, C. W.; Peanasky, M. J.; Drickamer, H. G. *J. Chem. Phys.* **1985**, *83*, 6108.

Table I. Physical Data for $[(\eta^6\text{-}C_6Me_6)_2Fe]^{2+}$–TCNQ Complexes

complex[a]	E_{app}, V vs SCE	ν_{CN}, cm^{-1}	conductivity, Ω^{-1} cm^{-1} [b]
1a	−0.10	2150, 2180	$<10^{-6}$
2a	+0.30	2200, 2182	1.0×10^{-1}
3a	+0.60	2177, 2194	$<10^{-6}$
4a	+0.48	2161, 2182	$<10^{-6}$
5a	+0.30	2160, 2182	1.0×10^{-2}
$[(\eta^6\text{-}C_6Me_6)_2Fe]$-$[TCNQ(OMe)_2]_x$	+0.05	2162, 2186	1.0×10^{-2}

[a] All compounds except **2** prepared in 0.1 M $[NBu_4][BF_4]$ nitromethane solutions containing 0.025 M TCNQ and 0.006 M $[(\eta^6\text{-}C_6Me_6)_2Fe][PF_6]_2$ at platinum electrodes. [b] Room-temperature conductivity measurements performed by four-point method with rectangular bars of pressed powders. The values reported are for the iron-containing complexes; the ruthenium analogues were identically prepared and exhibited identical physical characteristics.

against interconversion. It therefore seems unlikely that crystallization of **2** at +0.4 V involves **1** as an intermediate. Additionally, the selectivity toward either **1** or **2** at different potentials is obvious from the initial moments of crystallization as there is no visible observation of formation of both phases at the extreme potentials. When electrocrystallization was performed on large platinum foils, crystallization occurred on only a small area of the electrode, indicating favorable crystal growth on a relatively small number of nucleation sites. Under these conditions, the formation of both phases would have been obvious.

Substituent Effects in Electrocrystallization. Numerous derivatives of TCNQ are available that differ with respect to the electronic and steric properties of ring substituents. For example, the reduction potential becomes less positive with decreasing substituent electronegativity in the order $(TCNQ)F_4$ > $(TCNQ)Cl_2$ > TCNQ > $TCNQMe_2$. Accordingly, halogenated TCNQ phases $[(\eta^6\text{-}C_6Me_6)_2M][(TCNQ)F_4]_2$ (**3**) and $[(\eta^6\text{-}C_6Me_6)_2M][(TCNQ)Cl_2]_2$ (**4**) were prepared at potentials much more positive (Table I) than those used for **1** (eq 4 and 5). These

$$2(TCNQ)F_4 + 2e^- \xrightarrow{[(\eta^6\text{-}C_6Me_6)_2M]^{2+}} [(\eta^6\text{-}C_6Me_6)_2M][(TCNQ)F_4]_2 \quad (4)$$

3a, M = Fe
3b, M = Ru

$$2(TCNQ)Cl_2 + 2e^- \xrightarrow{[(\eta^6\text{-}C_6Me_6)_2M]^{2+}} [(\eta^6\text{-}C_6Me_6)_2M][(TCNQ)Cl_2]_2 \quad (5)$$

4a, M = Fe
4b, M = Ru

complexes grew as purple reflective crystals on the electrode surface and were easily harvested by filtration in Faradaic yields generally exceeding 90%. The multiphasic behavior observed for the TCNQ phases **1** and **2** was not evident for the complexes derived from the halogenated derivatives, as **3** and **4** were formed at all potentials studied in the range $+0.6 \geq E_{app} \geq -0.1$ V. The only apparent effect of crystallization at different potentials was more rapid crystal growth as E_{app} became more negative, which is due to more rapid generation of the anions. The positions of the ν_{CN} absorptions were substantially shifted to lower energy compared to those of $(TCNQ)F_4$ and $(TCNQ)Cl_2$ (ν_{CN} = 2215, 2226 and 2209, 2226 cm^{-1}, respectively) and were consistent with the presence of the fully reduced anions.

A pronounced difference was observed when electron-donating substituents were present on the TCNQ anions. When the same procedure was performed with $(TCNQ)Me_2$, only black needle-shaped crystals were formed, regardless of the applied potential. This compound was verified by elemental analysis and single-crystal X-ray studies (vide infra) to be $[(\eta^6\text{-}C_6Me_6)_2M]$-$[(TCNQ)Me_2]_3 \cdot 2CH_3NO_2$ (**5**). The ν_{CN} bands of **5** were shifted

$$3(TCNQ)Me_2 + 2e^- \xrightarrow{[(\eta^6\text{-}C_6Me_6)_2M]^{2+}} [(\eta^6\text{-}C_6Me_6)_2M][(TCNQ)Me_2]_3 \cdot 2CH_3NO_2 \quad (6)$$

5a, M = Fe
5b, M = Ru

Table II. Atomic Positional Parameters for **1a**[a]

atom	x	y	z
Fe	0.0000	0.0000	0.0000
N1	0.4752 (4)	0.7452 (4)	0.1139 (4)
N2	0.2531 (4)	0.8640 (4)	0.4970 (4)
N3	0.7369 (4)	0.5419 (4)	1.0278 (4)
N4	0.9788 (4)	0.4172 (4)	0.6564 (4)
C1	0.1990 (4)	0.0785 (3)	0.0092 (4)
C2	0.1853 (4)	0.0765 (3)	0.1596 (4)
C3	0.0801 (4)	0.1317 (3)	0.2343 (4)
C4	−0.0119 (4)	0.1919 (3)	0.1602 (4)
C5	0.0029 (4)	0.1953 (3)	0.0109 (4)
C6	0.1064 (4)	0.1376 (3)	−0.0661 (4)
C7	0.3155 (5)	0.0243 (5)	−0.0670 (6)
C8	0.2902 (5)	0.0215 (4)	0.2425 (6)
C9	0.0694 (5)	0.1326 (4)	0.3976 (5)
C10	−0.1196 (5)	0.2564 (4)	0.2444 (6)
C11	−0.0893 (5)	0.2677 (4)	−0.0621 (6)
C12	0.1255 (6)	0.1481 (4)	−0.2209 (5)
C13	0.5234 (4)	0.6805 (3)	0.4709 (5)
C14	0.6370 (4)	0.6229 (4)	0.4187 (4)
C15	0.7176 (4)	0.5728 (4)	0.5089 (5)
C16	0.6898 (4)	0.5745 (4)	0.6557 (5)
C17	0.5773 (4)	0.6327 (4)	0.7077 (4)
C18	0.4973 (4)	0.6830 (4)	0.6181 (4)
C19	0.4395 (4)	0.7362 (4)	0.3814 (4)
C20	0.4622 (4)	0.7395 (4)	0.2331 (5)
C21	0.3354 (4)	0.8058 (4)	0.4451 (4)
C22	0.7732 (4)	0.5219 (4)	0.7492 (5)
C23	0.7512 (4)	0.5319 (4)	0.9025 (5)
C24	0.8872 (4)	0.4639 (4)	0.6987 (5)
H1	0.347 (5)	−0.047 (4)	−0.046 (6)
H2	0.372 (5)	0.096 (4)	−0.051 (5)
H3	0.298 (5)	−0.010 (5)	−0.185 (5)
H4	0.249 (4)	−0.032 (4)	0.304 (5)
H5	0.302 (5)	−0.048 (5)	0.176 (6)
H6	0.337 (6)	0.080 (6)	0.339 (7)
H7	0.113 (5)	0.058 (5)	0.417 (6)
H8	0.135 (5)	0.203 (5)	0.487 (6)
H9	−0.015 (4)	0.120 (4)	0.401 (4)
H10	−0.093 (5)	0.349 (4)	0.283 (5)
H11	−0.194 (5)	0.269 (5)	0.165 (6)

[a] Estimated standard deviations in the least significant digits are shown in parentheses.

to lower frequency compared to those of $(TCNQ)Me_2$ (ν_{CN} = 2211, 2223 cm^{-1}), consistent with the presence of a reduced anion. The pressed-powder conductivity of **5** at room temperature was 1.0×10^{-2} Ω^{-1} cm^{-1}, and significant free carrier absorption was observed in the infrared region above 2000 cm^{-1}.

Similar results were obtained with $TCNQ(OMe)_2$, although it was difficult to verify the composition of the product owing to contamination by $TCNQ(OMe)_2$ that never fully dissolved in the electrochemical cell. The conductivity of the $TCNQ(OMe)_2$ product was similar (1×10^{-2} Ω^{-1} cm^{-1}) to that of **5**, although the accuracy of this value is questionable owing to the contamination. Electrocrystallization with TCNQ(Me)X (X = Cl, Br, I) derivatives afforded ill-characterized mixtures of both black crystals and reflective, purple crystals similar in appearance to the 1:2 phases described above. The inhomogeneity of these materials and their poor crystallinity precluded adequate characterization.

Structural Characterization. $[(\eta^6\text{-}C_6Me_6)_2M][TCNQ]_2$ (1a,b). Single-crystal X-ray diffraction revealed that **1a** and **1b** were isomorphous, crystallizing in the triclinic space group $P\bar{1}$ (Tables II and III). The unit cell of **1** consists of one cation and two anions, in which the metal atom of the cation lies on a crystallographic inversion center (Figure 1).

Although the $[(\eta^6\text{-}C_6Me_6)_2M]^{2+}$ cations have been extensively investigated with regard to their physical and electronic properties, with the exception of a recent report of the structure of $[(\eta^6\text{-}C_6H_6)_2Ru]^{2+}$,[18] structural characterization of this class of com-

(18) Beck, U.; Hummel, H.-B.; Ludi, A. *Organometallics* **1987**, *6*, 20.

Table III. Atomic Positional Parameters for **1b**[a]

atom	x	y	z
Ru	0.0000	0.0000	0.0000
N27	0.8880 (4)	0.5271 (4)	0.2571 (3)
N28	0.5059 (4)	0.7541 (4)	0.1372 (3)
N30	−0.0301 (4)	0.2661 (4)	0.4584 (3)
N31	0.3411 (4)	0.0193 (4)	0.5825 (3)
C1	0.1678 (4)	−0.0055 (4)	0.2013 (3)
C2	0.2430 (4)	0.0890 (4)	0.1388 (3)
C3	0.1628 (4)	0.1947 (4)	0.0829 (3)
C4	0.0133 (4)	0.2064 (4)	0.0843 (3)
C5	−0.0631 (4)	0.1117 (4)	0.1452 (3)
C6	0.0184 (4)	0.0079 (4)	0.2042 (3)
C11	0.2523 (5)	−0.1148 (4)	0.2639 (4)
C12	0.4004 (5)	0.0762 (5)	0.1354 (4)
C13	0.2459 (5)	0.2979 (4)	0.0241 (4)
C14	−0.0696 (5)	0.3192 (4)	0.0251 (4)
C15	−0.2185 (5)	0.1266 (5)	0.1521 (4)
C16	−0.0566 (5)	−0.0869 (4)	0.2744 (3)
C20	0.5289 (4)	0.4812 (4)	0.3207 (3)
C21	0.5825 (5)	0.3646 (4)	0.3775 (3)
C22	0.4896 (5)	0.2842 (4)	0.4275 (3)
C23	0.3437 (4)	0.3112 (4)	0.4257 (3)
C24	0.2899 (5)	0.4274 (4)	0.3679 (3)
C25	0.3824 (5)	0.5069 (4)	0.3173 (3)
C26	0.6220 (5)	0.5643 (4)	0.2655 (3)
C27	0.7685 (5)	0.5418 (4)	0.2630 (3)
C28	0.5579 (5)	0.6700 (4)	0.1958 (4)
C29	0.2478 (5)	0.2294 (4)	0.4792 (3)
C30	0.0960 (5)	0.2508 (4)	0.4685 (3)
C31	0.2997 (5)	0.1133 (4)	0.5372 (4)
H1	0.684 (6)	0.341 (5)	0.380 (4)
H2	0.514 (6)	0.212 (5)	0.455 (4)
H4	0.183 (6)	0.452 (5)	0.361 (4)
H5	0.346 (6)	0.579 (5)	0.282 (4)
H11A	0.345 (6)	−0.134 (5)	0.239 (4)
H11B	0.176 (6)	−0.201 (5)	0.254 (4)
H11C	0.258 (6)	−0.115 (5)	0.347 (4)
H12A	0.413 (6)	0.113 (5)	0.057 (4)
H12B	0.406 (5)	−0.007 (4)	0.121 (4)
H12C	0.482 (6)	0.126 (5)	0.205 (4)
H13A	0.319 (6)	0.268 (5)	−0.013 (4)
H13B	0.249 (6)	0.373 (5)	0.062 (4)
H13C	0.155 (6)	0.323 (5)	−0.058 (4)
H14A	−0.176 (6)	0.304 (5)	0.001 (4)
H14B	−0.032 (6)	0.347 (5)	−0.049 (4)
H14C	−0.037 (6)	0.396 (5)	0.086 (4)
H15A	−0.205 (6)	0.172 (5)	0.225 (4)
H15B	−0.278 (6)	0.161 (5)	0.082 (4)
H15C	−0.287 (6)	0.045 (5)	0.141 (4)
H16A	−0.169 (6)	−0.094 (5)	0.245 (4)
H16B	−0.050 (6)	−0.173 (5)	0.260 (4)
H16C	−0.042 (6)	−0.050 (5)	0.348 (4)

[a] Estimated standard deviations in the least significant digits are shown in parentheses.

Table IV. Bond Distances in $[(\eta^6\text{-}C_6Me_6)_2M]^{2+}$ (Å)[a]

Fe–C1	2.153 (4)	Ru–C1	2.262 (3)
Fe–C2	2.150 (4)	Ru–C2	2.257 (3)
Fe–C3	2.147 (4)	Ru–C3	2.254 (3)
Fe–C4	2.156 (4)	Ru–C4	2.250 (4)
Fe–C5	2.168 (4)	Ru–C5	2.256 (4)
Fe–C6	2.162 (4)	Ru–C6	2.261 (4)
C1–C2	1.416 (5)	C1–C2	1.452 (6)
C1–C6	1.418 (5)	C1–C6	1.406 (6)
C1–C7	1.501 (6)	C1–C7	1.499 (6)
C2–C3	1.400 (5)	C2–C3	1.427 (5)
C2–C8	1.506 (6)	C2–C8	1.481 (6)
C3–C4	1.416 (5)	C3–C4	1.397 (6)
C3–C9	1.515 (6)	C3–C9	1.519 (6)
C4–C5	1.415 (5)	C4–C5	1.446 (6)
C4–C10	1.492 (6)	C4–C10	1.510 (6)
C5–C6	1.401 (5)	C5–C6	1.427 (5)
C5–C11	1.509 (6)	C5–C11	1.482 (6)
C6–C12	1.507 (6)	C6–C12	1.512 (6)

[a] Estimated standard deviations in the least significant digits are shown in parentheses.

Table V. Bond Angles in $[(\eta^6\text{-}C_6Me_6)_2Fe]^{2+}$ (deg)[a]

C1–Fe–C2	38.4 (1)	C2–C1–C6	120.0 (4)
C1–Fe–C2	141.6 (1)	C2–C1–C7	120.1 (5)
C1–Fe–C3	69.3 (2)	C6–C1–C7	119.8 (4)
C1–Fe–C3	110.7 (2)	Fe–C2–C1	70.9 (2)
C1–Fe–C4	81.7 (1)	Fe–C2–C3	70.9 (2)
C1–Fe–C4	98.3 (1)	Fe–C2–C8	134.5 (3)
C1–Fe–C5	68.6 (2)	C1–C2–C3	120.4 (3)
C1–Fe–C5	111.4 (2)	C1–C2–C8	119.1 (5)
C1–Fe–C6	38.4 (1)	C3–C2–C8	120.4 (5)
C1–Fe–C6	141.6 (1)	Fe–C3–C2	71.1 (2)
C2–Fe–C3	38.0 (1)	Fe–C3–C4	71.1 (2)
C2–Fe–C3	142.0 (1)	Fe–C3–C9	132.9 (3)
C2–Fe–C3	68.9 (2)	C2–C3–C4	119.7 (3)
C2–Fe–C4	111.1 (2)	C2–C3–C9	119.8 (4)
C2–Fe–C5	81.3 (1)	C4–C3–C9	120.4 (4)
C2–Fe–C5	98.7 (1)	Fe–C4–C3	70.4 (2)
C2–Fe–C6	69.4 (1)	Fe–C4–C5	71.4 (2)
C2–Fe–C6	110.6 (1)	Fe–C4–C10	133.2 (3)
C3–Fe–C4	38.4 (1)	C3–C4–C5	119.8 (4)
C3–Fe–C4	141.6 (1)	C3–C4–C10	119.4 (4)
C3–Fe–C5	69.2 (1)	C5–C4–C10	120.0 (4)
C3–Fe–C5	110.8 (1)	Fe–C5–C4	70.4 (2)
C3–Fe–C6	82.3 (1)	Fe–C5–C6	70.9 (2)
C3–Fe–C6	97.7 (1)	Fe–C5–C11	134.9 (3)
C4–Fe–C5	38.2 (1)	C4–C5–C6	120.7 (3)
C4–Fe–C5	141.8 (1)	C4–C5–C11	119.5 (5)
C4–Fe–C6	69.1	C6–C5–C11	119.7 (4)
C4–Fe–C6	110.9 (1)	Fe–C6–C1	70.5 (2)
C5–Fe–C6	37.8 (1)	Fe–C6–C5	71.4 (2)
C5–Fe–C6	142.2 (1)	Fe–C6–C12	134.7 (3)
Fe–C1–C2	70.7 (2)	C1–C6–C5	119.3 (3)
Fe–C1–C6	71.1 (2)	C1–C6–C12	120.3 (5)
Fe–C1–C7	133.7 (3)	C5–C6–C12	120.2 (4)

[a] Estimated standard deviations in the least significant digits are shown in parentheses.

Table VI. Bond Angles in $[(\eta^6\text{-}C_6Me_6)_2Ru]^{2+}$ (deg)[a]

C1–Ru–C2	142.5 (1)	C2–C1–C6	119.8 (3)
C1–Ru–C2	37.5 (1)	C2–C1–C7	119.2 (4)
C1–Ru–C3	113.6 (1)	C6–C1–C7	121.0 (4)
C1–Ru–C3	66.4 (1)	Ru–C2–C1	71.4 (2)
C1–Ru–C4	101.6 (1)	Ru–C2–C3	71.5 (2)
C1–Ru–C4	78.4 (1)	Ru–C2–C8	129.3 (3)
C1–Ru–C5	113.7 (1)	C1–C2–C3	118.5 (4)
C1–Ru–C5	66.3 (1)	C1–C2–C8	120.2 (4)
C1–Ru–C6	143.8 (2)	C3–C2–C8	121.3 (4)
C1–Ru–C6	36.2 (2)	Ru–C3–C2	71.7 (2)
C2–Ru–C3	143.1 (1)	Ru–C3–C4	71.8 (2)
C2–Ru–C3	36.9 (1)	Ru–C3–C9	131.4 (3)
C2–Ru–C4	113.7 (1)	C2–C3–C4	121.6 (4)
C2–Ru–C4	66.3 (1)	C2–C3–C9	118.3 (4)
C2–Ru–C5	100.9 (1)	C4–C3–C9	120.1 (4)
C2–Ru–C5	79.1 (1)	Ru–C4–C3	72.1 (2)
C2–Ru–C6	113.6 (1)	Ru–C4–C5	71.5 (2)
C2–Ru–C6	66.4 (1)	Ru–C4–C10	130.0 (2)
C3–Ru–C4	143.9 (2)	C3–C4–C5	120.2 (3)
C3–Ru–C4	36.1 (2)	C3–C4–C10	120.8 (4)
C3–Ru–C5	113.7 (1)	C5–C4–C10	118.9 (4)
C3–Ru–C5	66.3 (1)	Ru–C5–C4	71.0 (2)
C3–Ru–C6	102.4 (1)	Ru–C5–C6	71.8 (2)
C3–Ru–C6	77.6 (1)	Ru–C5–C11	131.4 (2)
C4–Ru–C5	142.6 (2)	C4–C5–C6	118.5 (4)
C4–Ru–C5	37.4 (2)	C4–C5–C11	120.7 (4)
C4–Ru–C6	113.6 (1)	C6–C5–C11	120.8 (4)
C4–Ru–C6	66.4 (1)	Ru–C6—C1	71.9 (2)
C5–Ru–C6	143.2 (1)	Ru–C6–C5	71.4 (2)
C5–Ru–C6	36.8 (1)	Ru–C6–C12	131.6 (2)
Ru–C1–C2	71.1 (2)	C1–C6–C5	121.5 (4)
Ru–C1–C6	71.8 (2)	C1–C6–C12	119.7 (4)
Ru–C1–C7	130.2 (3)	C5–C6–C12	118.8 (4)

[a] Estimated standard deviations in the least significant digits are shown in parentheses.

plexes has not been reported. The bond distances and angles for the $[(\eta^6\text{-}C_6Me_6)M]^{2+}$ cations in **1a** and **1b**, which are illustrative of the molecular structure of the cations in **3a,b** and **4a,b** are given

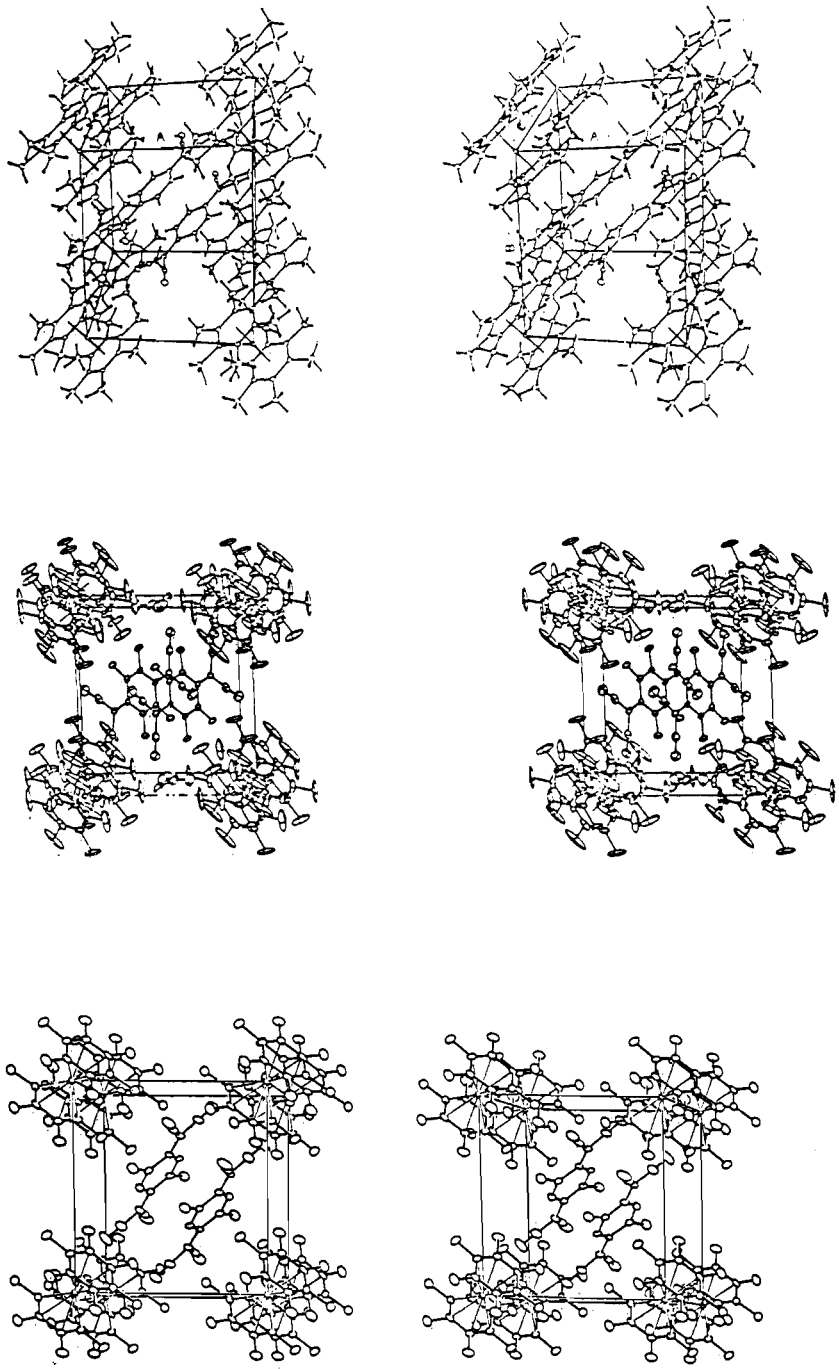

Figure 1. Stereoviews of the 1:2 phases **1a**, **3a**, and **4a** (from top to bottom) drawn with 50% ellipsoids.

Table VII. Structural Features of the 1:2 TCNQ Complexes

compd	dist between C_6Me_6 planes, Å	dist between intradimer TCNQ planes, Å	intradimer dihedral TCNQ–TCNQ angle, deg	dihedral TCNQ–C_6Me_6 angle, deg	M–M intrastack dist, Å
1a	3.276	3.24	0.21	1.9	14.31
3a	3.232	3.17	0.29	95.4	18.53
4a	3.232	3.21	2.17	87.2	18.68
1b	3.518	3.23	0.43	2.9	14.44
3b	3.465	3.14	0.29	84.2	18.65
4b	3.445	3.22	0.00	93.1	18.82

in Tables IV–VI. The expected "sandwich" structure is observed (Figure 2) as the ring planes are nominally parallel with only very small dihedral angles between the rings (**1a**, 0.73°; **1b**, 0.85°). The rings are eclipsed with respect to the methyl groups. We have observed this geometry for all $[(\eta^6\text{-}C_6Me_6)M]^{2+}$ cations with the exception of the dithiolate complex $[(\eta^6\text{-}C_6Me_6)Fe][Fe\{C_2S_2(CN)_2\}_2]\cdot 2CH_3NO_2$, which exhibits a staggered conformation of the methyl groups.[19] The distance between the rings (d_{Ar-Ar}) is larger for **1b** owing to the larger radius of ruthenium compared to that of iron (Table VII). The average M–C(ring) distances in **1a** and **1b** are 2.156 and 2.257 Å, respectively, and only very small deviations out of the plane are observed for the ring carbons. Likewise, the methyl carbons do not show any significant bending

(19) Ward, M. D., unpublished results.

Table VIII. Average Bond Lengths (Å) for TCNQ Complexes

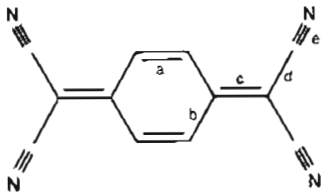

compds	*a*	*b*	*c*	*d*	*e*	d_{C-Cl}	d_{C-F}
$[Fe(\eta^6\text{-}C_6Me_6)_2][TCNQ]_2$ (**1a**)	1.361 (6)	1.405 (6)	1.419 (5)	1.417 (6)	1.141 (6)		
$[Ru(\eta^6\text{-}C_6Me_6)_2][TCNQ]_2$ (**1b**)	1.374 (6)	1.414 (6)	1.428 (6)	1.415 (6)	1.151 (6)		
TCNQ[28]	1.346 (3)	1.448 (4)	1.374 (3)	1.441 (4)	1.140 (1)		
RbTCNQ[27]	1.373 (1)	1.423 (3)	1.420 (1)	1.416 (8)	1.153 (7)		
$[Pt(NH_3)_4]^{2+}[TCNQ]_2^{2-}$ [26]	1.345 (10)	1.42	1.40 (1)	1.41 (2)	1.14 (2)		
$[Fe(\eta^6\text{-}C_6Me_6)_2][(TCNQ)F_4]_2$ (**3a**)	1.352 (9)	1.408 (9)	1.385 (9)	1.425 (9)	1.144 (10)		1.363 (7)
$[Ru(\eta^6\text{-}C_6Me_6)_2][(TCNQ)F_4]_2$ (**3b**)	1.373 (9)	1.392 (9)	1.441 (9)	1.412 (10)	1.145 (10)		1.338 (8)
$(TCNQ)F_4$[31]	1.334	1.437	1.372	1.437	1.140		1.337 (1)
$[Me_2\text{-phyz}]^+[(TCNQ)F_4]^{-a}$	1.353	1.415	1.415	1.429	1.144		1.354 (4)
$[5\text{-}n\text{-Bu-phz}]_2^{2+}[(TCNQ)F_4]_2^{2-}$ [29]	1.350	1.410	1.413	1.417	1.144		1.346 (4)
$[Fe(\eta^6\text{-}C_6Me_6)_2][(TCNQ)Cl_2]_2$ (**4a**)	1.35 (2)	1.41 (2)	1.405 (2)	1.45 (2)	1.14 (2)	1.69 (1)	
$[Ru(\eta^6\text{-}C_6Me_6)_2][(TCNQ)Cl_2]_2$ (**4b**)	1.38 (1)	1.40 (1)	1.44 (1)	1.40 (1)	1.16 (1)	1.69 (1)	
$[DBTTF][(TCNQ)Cl_2]$[33,b]	1.352	1.436	1.391	1.433	1.137	1.726	

[a] Soos, Z. G.; Keller, H. J.; Luidof, K.; Queckborner, J.; Weke, D.; Flandrois, S. *J. Chem. Phys.* **1981**, *76*, 5287. [b] Abbreviations: Me_2-phz = dimethylphenazinium; 5-*n*-Bu-phz = 5-*n*-butylphenazinium; DBTTF = dibenzotetrathiafulvalene.

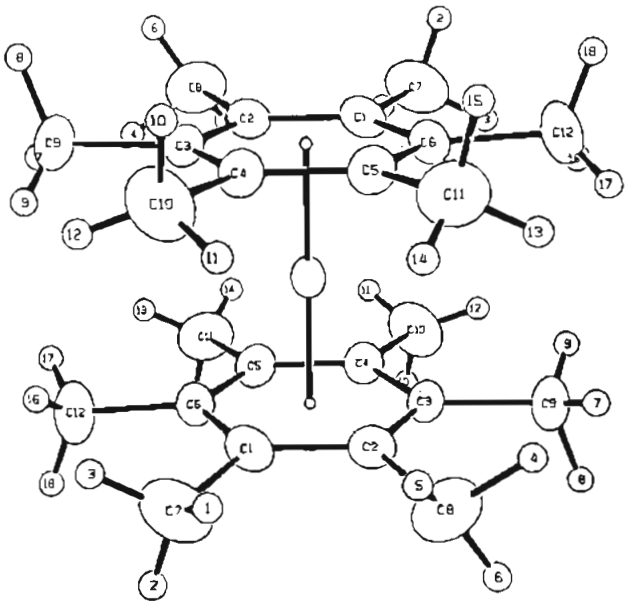

Figure 2. Numbering scheme for the $[(\eta^6\text{-}C_6Me_6)_2M]^{2+}$ cation.

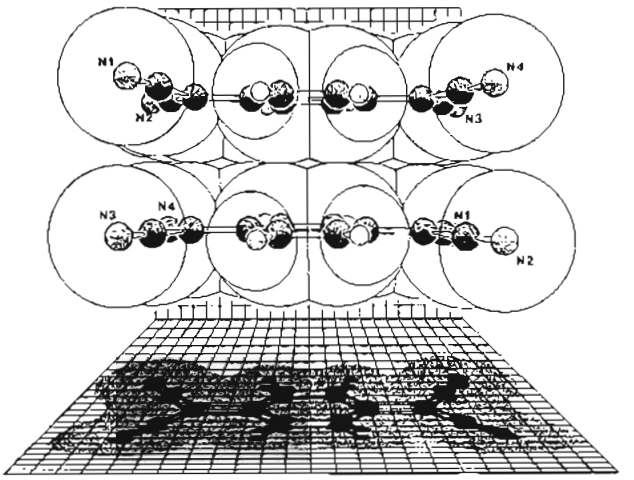

Figure 3. Representation of the $[TCNQ]_2^{2-}$ dimer dianion of **1** as viewed 20 Å from the center of mass of the dimer. Each division of the grid is equivalent to 0.5 Å. The numbering scheme for the nitrogen atoms is used for $[(TCNQ)F_4]_2^{2-}$ in **3**. The drawing was made with the KANVAS program, based on the program SCHAKAL by E. Keller (Kristallographisches Institute der Universität Freiburg, Frieburg, FRG), which was modified by A. J. Arduengo, III (E. I. du Pont de Nemours& Co., Wilmington, DE), to produce the back and shadowed planes. The planes bear a 50-pm grid, and the lighting source is at infinity so that the shadow size is meaningful.

out of the ring plane. The average C–C(ring) bond distances are 1.411 and 1.426 Å for **1a** and **1b**, respectively, and the C(ring)–C(methyl) bond distances are 1.505 and 1.501 Å. These values are near those claimed for hexamethylbenzene alone,[20] which are C–C(ring) = 1.39 Å and C(ring)–C(methyl) = 1.53 Å. Space-filling models show that the metal atoms of the cations are essentially obscured by the hydrocarbon framework, which excludes direct interactions between metal atoms and anions in these phases.

The anions lie on general positions and exist as a $[TCNQ]_2^{2-}$ dimer (Figure 3) located in the center of the triclinic unit cell. The intradimer separation between $TCNQ^-$ planes was essentially the same for both **1a** and **1b** (Table VII) and is significantly less than the generally accepted 3.5–3.6-Å van der Waals separation.[21–23] The ring planes are essentially parallel with only small dihedral angles of 0.21 and 0.43° for **1a** and **1b**, respectively. The dimer exhibits the commonly observed[24] ring–ring overlap with one of the rings slipped approximately 0.60 Å along the short axis of the TCNQ anion. This extent of slippage is similar to that observed for the discrete dimers present in $[(\eta^5\text{-}C_5Me_5)Fe]_2[TCNQ]_2$,[2] $Nb_3Cl_6(C_6Me_6)_3(TCNQ)_2$,[25] and $[Pt(NH_3)_4][TCNQ]_2$.[26] The anions are slightly boat-shaped with the $C(CN)_2$ planes bent from the TCNQ ring plane in a direction away from the dimer. The $C(CN)_2$ planes form angles of 3.87 and 7.78° with the ring plane in **1a** and 4.64 and 7.30° in **1b**. As a result,

(20) Brockway, L. O.; Robertson, J. M. *J. Chem. Soc.* **1939**, 1324.
(21) Soos, Z. G. *Annu. Rev. Phys. Chem.* **1974**, *25*, 121.
(22) Offen, H. W. *J. Chem. Phys.* **1965**, *42*, 430.
(23) Mayerle, J. J.; Torrance, J. B.; Crowley, J. I. *Acta Crystallogr., Sect. B: Struct. Crystallogr. Cryst. Chem.* **1979**, *B35*, 2988.
(24) Endres, H. In *Extended Linear Chain Compounds*; Miller, J. S., Ed.; Plenum: New York, 1983; Vol. 3, p 263, and references therein.
(25) Goldberg, S. Z.; Spivack, B.; Stanley, G.; Eisenberg, R.; Braitsch, D. M.; Miller, J. S.; Abkowitz, M. *J. Am. Chem. Soc.* **1977**, *99*, 110.
(26) Endres, H.; Keller, H. J.; Moroni, W.; Nöthe, D.; Dong, V. *Acta Crystallogr., Sect. B: Struct. Crystallogr. Cryst. Chem.* **1978**, *B34*, 1703.

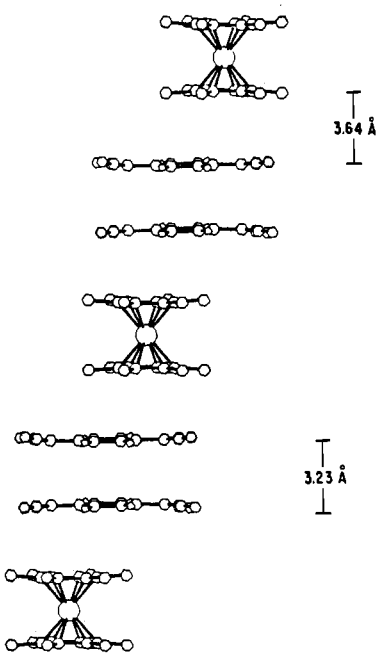

Figure 4. Illustration of a single 1-D mixed ...DAADAA... stack in **1a**,**b**. Note that the quinoid portions of the TCNQ anions overlap the arene ligands, resulting in a "stepped" motif. Hydrogen atoms have been omitted for clarity.

the methylidene carbon atoms lie out of the ring plane by 0.01–0.03 Å. This slipped arrangement allows for some overlap of the out-of-plane b_{3g} π orbitals, which contain the unpaired electron of each anion, while alleviating Coulombic repulsion. The average bond distances for the $TCNQ^-$ anions (Table VIII) are consistent with values previously reported, e.g. for RbTCNQ,[27] and are readily distinguished from the bond lengths in TCNQ.[28]

The cations (D) and dimer dianions (AA) form extended mixed-stack linear chains (Figure 4), i.e. ...DAADAADAA..., which do not coincide closely with any of the crystallographic axes. The distance between the $TCNQ^-$ plane and its neighboring hexamethylbenzene plane for **1a** and **1b** are 3.64 and 3.60 Å, respectively, suggesting only weak van der Waals interactions. The intermolecular N(cyano)–H(methyl) distances fall in the range 2.45–3.48 Å; those at the low end of this range may be indicative of weak hydrogen-bonding interactions. The methylidene ends of the dimer approach the arene ligands more closely than the quinoid portion of the anion, with opposite ends of the dimer associated with the two neighboring cations. This arrangement gives the linear chain a "stepped" motif, with the M–M vectors forming angles with the anion planes of 73.53 and 73.37° in **1a** and **1b**. When this arrangement is viewed with translation along the *c* axis, "sheets" of anions interleaved between cations are observed. There are no extraordinary interstack interactions between either the TCNQ anions or the cations, although an interstack contact of 3.57 Å between nitrogens of $TCNQ^-$ anions within these sheets is observed.

$[(\eta^6\text{-}C_6Me_6)_2M_I(TCNQ)F_4]_2$ (3a,b). The 1:2 phase formed by electrochemical reduction of $(TCNQ)F_4$ in the presence of $[(\eta^6\text{-}C_6Me_6)M]^{2+}$ cations also crystallized in the $P\bar{1}$ (Tables IX and X) space group and contained a $[(TCNQ)F_4]_2^{2-}$ dimer dianion in the center of the triclinic unit cell. The dimer dianion exhibits ring–ring overlap with an intradimer separation (3.17 Å) which is significantly less than that for the $[TCNQ]_2^{2-}$ dimer in **1a**,**b**. This distance is similar to that reported for [5-*n*-Bu-phz]-$[(TCNQ)F_4]$[29] (5-*n*-Bu-phz = 5-*n*-butylphenazinium) but shorter than the 3.27-Å separation reported for $[HMTTF][(TCNQ)F_4]$[30] (HMTTF = hexamethylenetetrathiafulvalene) (the dimer in [5-*n*-Bu-phz]$[(TCNQ)F_4]$ actually exhibits a ring over exocyclic bond overlap instead of the ring–ring overlap observed in **3**). The $(TCNQ)F_4^-$ bond distances are in good agreement with those previously observed (Table VIII). The exocyclic methylidene bond

Table IX. Atomic Positional Parameters for **3a**[a]

atom	*x*	*y*	*z*
Fe	0.000 (0)	0.000 (0)	0.000 (0)
F1	0.5516 (5)	0.3382 (4	0.2717 (5)
F2	0.3907 (5)	0.2595 (4)	0.4395 (5)
F3	0.2081 (5)	0.6530 (4)	0.4926 (6)
F4	0.3723 (5)	0.7322 (4)	0.3253 (6)
O1	−0.503 (2)	−0.016 (2)	−0.360 (2)
O2	0.642 (2)	0.026 (2)	0.508 (3)
N1	0.0326 (8)	0.5349 (9)	0.6909 (9)
N2	0.1716 (9)	0.1825 (8)	0.6110 (10)
N3	0.7035 (9)	0.4493 (9)	0.0481 (9)
N4	0.5777 (9)	0.8032 (8)	0.1341 (10)
C1	0.0014 (9)	−0.0832 (10)	0.1828 (10)
C2	−0.0698 (11)	0.0234 (10)	0.1988 (9)
C3	−0.1713 (10)	0.0378 (9)	0.1055 (10)
C4	−0.2049 (9)	−0.0495 (12)	−0.0015 (10)
C5	−0.1386 (10)	−0.1540 (10)	−0.0156 (10)
C6	−0.0358 (10)	−0.1749 (8)	0.0756 (11)
C7	0.1126 (13)	−0.0995 (17)	0.2881 (14)
C8	−0.0436 (21)	0.1200 (15)	0.3131 (13)
C9	−0.2591 (14)	0.1520 (13)	0.1220 (18)
C10	−0.3228 (12)	−0.0335 (20)	−0.1001 (16)
C11	−0.1823 (17)	−0.2517 (16)	−0.1292 (17)
C12	0.0331 (15)	−0.2971 (11)	0.0597 (20)
C13	0.4655 (8)	0.4188 (8)	0.3240 (9)
C14	0.3818 (8)	0.3794 (7)	0.4121 (9)
C15	0.2892 (8)	0.4510 (8)	0.4778 (9)
C16	0.2944 (8)	0.5726 (8)	0.4393 (9)
C17	0.3782 (8)	0.6121 (8)	0.3520 (9)
C18	0.4700 (8)	0.5416 (7)	0.2872 (8)
C19	0.2042 (8)	0.4095 (8)	0.5669 (9)
C20	0.1106 (9)	0.4824 (9)	0.6351 (9)
C21	0.1899 (9)	0.2843 (9)	0.5899 (10)
C22	0.5590 (8)	0.5824 (8)	0.1997 (9)
C23	0.6400 (9)	0.5042 (9)	0.1174 (9)
C24	0.5660 (9)	0.7051 (9)	0.1665 (10)
C25	0.5499 (1)	0.0158 (12)	0.4614 (15)

[a] Estimated standard deviations in the least significant digits are shown in parentheses.

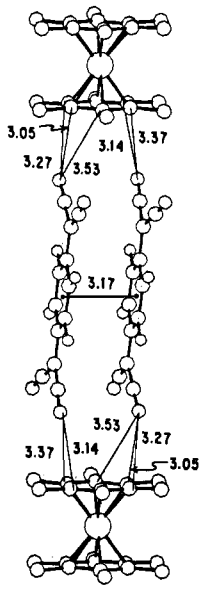

Figure 5. Intermolecular bond distances in **3a**. Hydrogen atoms have been omitted for clarity.

(27) Hoekstra, A.; Spoelder, T.; Vos, A. *Acta Crystallogr., Sect. B: Struct. Crystallogr. Cryst. Chem.* **1972**, *B28*, 14.
(28) Long, R. E.; Sparks, R. A.; Trueblood, K. N. *Acta Crystallogr.* **1965**, *18*, 932.
(29) Harms, R. H.; Keller, H. J.; Nothe, D.; Wehe, D.; Heimer, N.; Metzger, R. M.; Gundel, D.; Sixl, H. *Mol. Cryst. Liq. Cryst.* **1982**, *85*, 249.
(30) Torrance, J. B.; Mayerle, J. J.; Bechgaard, K.; Silverman, B. D.; Tomkiewicz, Y. *Phys. Rev. B: Condens. Matter* **1980**, *22*, 4960.

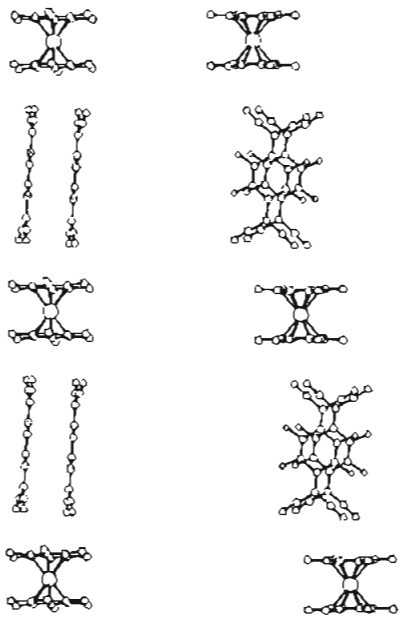

Figure 6. Illustrations of a single 1-D mixed ...DAADAA... stack in **3a** viewed parallel and perpendicular to the planes of the $[(TCNQ)F_4]_2^{2-}$ dimer dianion. Hydrogen atoms have been omitted for clarity.

length is significantly longer than that in $(TCNQ)F_4$,[31] in accordance with predictions of decreased bond order in the anion.[32]

One-dimensional linear chains with mixed ...DAADAADAA... stacks of $[(\eta^6\text{-}C_6Me_6)M]^{2+}$ cations (D) and $[(TCNQ)F_4]_2^{2-}$ (AA) dimer dianions are also observed for these complexes. However, an unusual motif is observed in which the long axis of the $[(TCNQ)F_4]_2^{2-}$ dimer is nearly perpendicular to the hexamethylbenzene planes of the cations (Figures 5 and 6). The linear-chain axes as defined by the M–M vectors form angles of 7.66 and 6.48° with the planes of $[(TCNQ)F_4]_2^{2-}$ for **3a** and **3b**, respectively. Consequently, the anion planes are nearly coincident with the linear chains.

This unique arrangement results in several very close intermolecular contacts between nitrogen atoms of the $[(TCNQ)F_4]_2^{2-}$ moiety and the ring carbons of the cation, implying a σ interaction of the nitrogen atoms with the π-system of the hexamethylbenzene ligands. For example, **3a** exhibits N2–C1, N2–C6, and N4–C4 contact distances of 3.05, 3.27, and 3.14 Å, respectively (see the numbering scheme for $[TCNQ]_2^{2-}$ in Figure 3). Likewise, **3b** possesses contacts of 3.04, 3.21, and 3.10 Å between the same sets of atoms. Therefore, nitrogen atoms from both $TCNQ^-$ anions of the dimer are involved in these interactions. These are related to an equivalent set of interactions with a cation on the opposite side of the dimer by an inversion center as necessitated by the crystallographic space group.

Although the individual stacks are essentially discrete in nature, there are interstack contacts of 3.47 and 3.43 Å between C–N nitrogens and fluorine atoms in stacks related by translation along the *c* axis. In addition, stacks related by translation along the *a* axis possess $[(TCNQ)F_4]_2^{2-}$ groups whose planes are slipped along the long molecular axis and are parallel. However, interaction between these species is negligible as the interdimer distance is >3.8 Å.

$[(\eta^6\text{-}C_6Me_6)_2M][(TCNQ)Cl_2]_2$ (4a,b). The 1:2 phases with $(TCNQ)Cl_2$ also crystallized in the $P\bar{1}$ (Tables XI and XII) space group with a $[(TCNQ)Cl_2]_2^{2-}$ dimer located in the center of the triclinic cell, with an intradimer separation of 3.21 Å. The $C(CN)_2$ planes bend away from the ring and are significantly twisted about the long axis of the molecule by 8.86° (N3,N4 plane) and 6.10° (N1,N2 plane). This distortion is most likely due to steric interactions with the Cl atoms on the ring. Indeed, several close

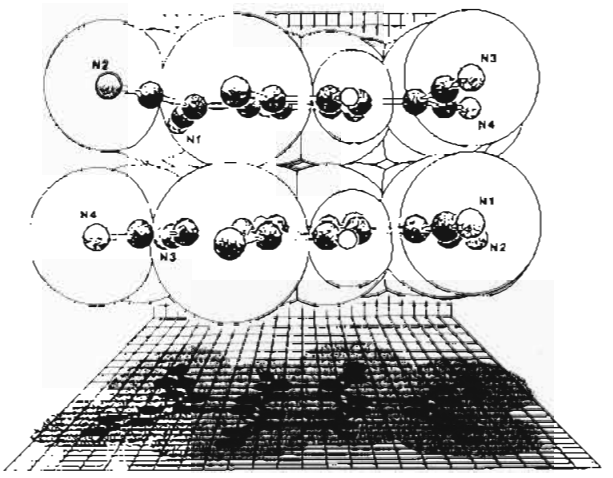

Figure 7. Representation of the $[(TCNQ)Cl_2]_2^{2-}$ dimer dianion of **4a** as viewed 20 Å from the center of mass of the dimer. Each division of the grid is equivalent to 0.5 Å. The drawing was made with the KANVAS program (see caption to Figure 3).

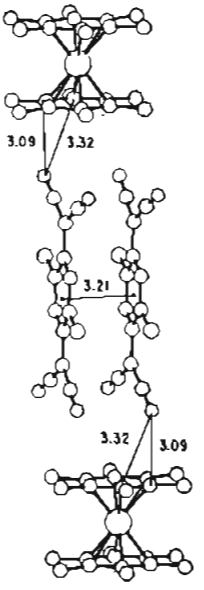

Figure 8. Intermolecular bond distances in **4a**. Hydrogen atoms have been omitted for clarity.

nonbonded contacts are observed between nitrogen and chlorine (N2–Cl1 = 3.36 Å, N4–Cl2 = 4.43 Å) and particularly between carbon atoms and chlorine (C24–Cl2 = 2.98 Å, C21–Cl1 = 2.96 Å). The bond lengths and angles and overlap pattern of the anions are similar to those reported for the segregated stack complex [DBTTF][$(TCNQ)Cl_2$][33] (DBTTF = dibenzotetrathiafulvalene); however, **4a,b** exhibit smaller intradimer separations. Although two different overlap patterns are possible for this dianion, only the "meso" form where C–Cl bonds are nominally eclipsed (Figure 7) is observed, and as a result the unit cell is not chiral (the staggered arrangement would result in a chiral unit cell since the mirror image of the dimer dianion is not superimposable in this case). This arrangement is reminiscent of molecular packing commonly observed in chloro aromatic compounds, where the "attractive nature" of Cl–Cl interactions has been proposed to exert a strong influence on the crystal structure.[34] For example, 2,6-dichlorocinnamic acid exhibits an intermolecular overlap motif which is similar to that of the $[(TCNQ)Cl_2]_2^{2-}$ dimer.

In a fashion similar to that of **3**, a mixed-stack ...DAADAADAA... motif is observed with the $[(TCNQ)Cl_2]_2^{2-}$ dimer planes

(31) Emge, T. J.; Maxfield, M.; Cowan, D. O.; Kistenmacher, T. J. *Mol. Cryst. Liq. Cryst.* **1981**, *65*, 161.
(32) Dixon, D. A., unpublished results.
(33) Soling, H.; Rindorf, G.; Thorup, N. *Acta Crystallogr., Sect. B: Struct. Crystallogr. Cryst. Chem.* **1981**, *B37*, 1716.
(34) Sarma, J. A. R. P.; Desiraju, G. R. *Acc. Chem. Res.* **1986**, *19*, 222 and references therein.

Table X. Atomic Positional Parameters for **3b**[a]

atom	x	y	z
Ru	0.0000	0.0000	0.0000
F1	0.5585 (3)	−0.3933 (3)	−0.2604 (3)
F2	0.7245 (3)	−0.5525 (3)	−0.3386 (3)
F3	0.6752 (4)	−0.3690 (3)	−0.7330 (3)
F4	0.5095 (4)	−0.2080 (3)	−0.6552 (3)
N27	0.3944 (6)	−0.1759 (5)	−0.1811 (6)
N28	0.3084 (6)	−0.0383 (5)	−0.5388 (6)
N30	0.9500 (6)	−0.7004 (6)	−0.4475 (6)
N31	0.8622 (7)	−0.5711 (6)	−0.8065 (6)
C1	0.1894 (6)	−0.0042 (5)	−0.0881 (7)
C2	0.0823 (7)	−0.0367 (6)	−0.1814 (6)
C3	−0.0111 (6)	−0.1404 (6)	−0.1658 (6)
C4	−0.0020 (6)	−0.2132 (6)	−0.0589 (7)
C5	0.1046 (7)	−0.1863 (6)	0.0321 (6)
C6	0.2016 (6)	−0.0822 (7)	0.0179 (6)
C11	0.2974 (8)	0.1057 (8)	−0.094 (1)
C12	0.079 (1)	0.042 (1)	−0.2952 (8)
C13	−0.122 (1)	−0.173 (1)	−0.272 (1)
C14	−0.1089 (9)	−0.3250 (7)	−0.049 (1)
C15	0.113 (1)	−0.2734 (8)	0.1434 (9)
C16	0.3177 (8)	−0.057 (1)	0.122 (1)
C20	0.5247 (5)	−0.2906 (5)	−0.4534 (5)
C21	0.5865 (5)	−0.3839 (5)	−0.3775 (5)
C22	0.6744 (5)	−0.4668 (5)	−0.4189 (5)
C23	0.7097 (5)	−0.4692 (5)	−0.5396 (5)
C24	0.6482 (5)	−0.3758 (5)	−0.6161 (5)
C25	0.5610 (5)	−0.2925 (5)	−0.5729 (5)
C26	0.4334 (5)	−0.2055 (5)	−0.4078 (5)
C27	0.4122 (6)	−0.1921 (5)	−0.2823 (5)
C28	0.3663 (6)	−0.1140 (6)	−0.4848 (6)
C29	0.7994 (5)	−0.5570 (5)	−0.5849 (5)
C30	0.8792 (6)	−0.6362 (6)	−0.5050 (6)
C31	0.8318 (6)	−0.5614 (6)	−0.7081 (6)
O1	0.530 (2)	0.647 (2)	0.024 (2)
O2	0.348 (2)	0.493 (2)	0.012 (2)
C	0.4584 (9)	0.5523 (9)	0.0147 (9)
N	0.458	0.552	0.015
H11A	0.280	0.153	−0.169
H11B	0.300	0.167	−0.021
H11C	0.384	0.068	−0.092
H12A	−0.001	0.007	−0.352
H12B	0.072	0.132	−0.274
H12C	0.157	0.028	−0.336
H13A	−0.180	−0.247	−0.250
H13B	−0.172	−0.097	−0.286
H13C	−0.083	−0.197	−0.346
H14A	−0.090	−0.366	0.030
H14B	−0.196	−0.289	−0.052
H14C	−0.109	−0.390	−0.117
H15A	0.194	−0.242	0.199
H15B	0.036	−0.266	0.187
H15C	0.121	−0.363	0.116
H16A	0.377	0.017	0.100
H16B	0.283	−0.036	0.199
H16C	0.367	−0.135	0.129

[a] Estimated standard deviations in the least significant digits are shown in parentheses.

almost perpendicular to the hexamethylbenzene ligand planes, accompanied by close intermolecular contacts between N4 of the anions and ring carbons C1 and C2 (Figures 8 and 9). For example, N4 of **4a** is located 3.09 Å from C1 of the hexamethylbenzene ring and 3.31 Å from C2. The ruthenium analogue **4b** also exhibits similar behavior, although the nitrogen atom of the anion is located 3.09 Å from C3 and 3.39 Å from both C2 and C4. Each anion in the dimer therefore possesses one nitrogen atom in very close proximity to the hexamethylbenzene ring of the cations. The linear-chain axes as defined by the M–M vectors form angles of 16.04 and 16.24° with the planes of $[(TCNQ)Cl_2]_2^{2-}$ for **4a** and **4b**, respectively. Interstack contacts of 3.52 and 3.55 Å between C–N nitrogens and chlorine atoms between stacks related by translation along the *c* axis are present, indicating minimal interstack interactions.

Other Phases. Unfortunately, single crystals of the conducting phases **2a,b** were plagued by disorder and facile solvent loss, which

Table XI. Atomic Positional Parameters for **4a**[a]

atom	x	y	z
Fe	0	0	0
Cl1	−0.7477 (4)	0.3933 (4)	0.7279 (5)
Cl2	−0.5385 (4)	0.4147 (4)	0.1613 (4)
N1	−0.355 (1)	0.079 (1)	0.459 (1)
N2	−0.535 (1)	0.190 (1)	0.836 (1)
N3	−0.921 (2)	0.736 (2)	0.452 (2)
N4	−0.763 (2)	0.619 (1)	0.054 (1)
C1	−0.058 (2)	0.189 (1)	0.059 (2)
C2	−0.174 (1)	0.115 (1)	0.033 (2)
C3	−0.204 (1)	0.019 (1)	−0.097 (2)
C4	−0.114 (2)	0.006 (1)	−0.202 (1)
C5	0.004 (1)	0.083 (1)	−0.177 (2)
C6	0.033 (1)	0.179 (1)	−0.044 (2)
C7	−0.034 (2)	0.293 (1)	0.196 (2)
C8	−0.278 (2)	0.137 (2)	0.138 (2)
C9	−0.332 (2)	−0.057 (2)	−0.124 (2)
C10	−0.153 (2)	−0.093 (2)	−0.341 (2)
C11	0.093 (2)	0.068 (1)	−0.286 (2)
C12	0.149 (2)	0.265 (2)	−0.017 (2)
C13	−0.573 (1)	0.322 (1)	0.527 (1)
C14	−0.682 (1)	0.399 (1)	0.574 (1)
C15	−0.736 (1)	0.482 (1)	0.502 (2)
C16	−0.696 (1)	0.498 (1)	0.375 (2)
C17	−0.596 (1)	0.413 (1)	0.323 (1)
C18	−0.539 (1)	0.333 (1)	0.397 (1)
C19	−0.510 (1)	0.236 (1)	0.596 (2)
C20	−0.420 (2)	0.151 (1)	0.523 (2)
C21	−0.530 (2)	0.212 (1)	0.730 (2)
C22	−0.761 (2)	0.586 (2)	0.309 (2)
C23	−0.854 (2)	0.671 (2)	0.387 (2)
C24	−0.754 (2)	0.601 (1)	0.166 (2)
H1	−0.037	0.262	0.278
H2	−0.103	0.356	0.195
H3	0.052	0.336	0.206
H4	−0.277	0.222	0.188
H5	−0.368	0.112	0.091
H6	−0.258	0.089	0.210
H7	−0.409	−0.017	−0.167
H8	−0.326	−0.137	−0.186
H9	−0.356	−0.067	−0.034
H10	−0.222	−0.075	−0.412
H11	−0.075	−0.117	−0.390
H12	−0.186	−0.169	−0.321
H13	0.164	0.132	−0.263
H14	0.139	−0.010	−0.298
H15	0.044	0.069	−0.378
H16	0.189	0.288	0.080
H17	0.220	0.229	−0.074
H18	0.128	0.342	−0.046
H19	−0.804	0.533	0.542
H20	−0.470	0.282	0.357

[a] Estimated standard deviations in the least significant digits are shown in parentheses.

prevented satisfactory X-ray structural analysis. However, the poorly refined data (R = 0.40) did indicate the presence of one-dimensional extended TCNQ stacks adjacent to the $[(\eta^6\text{-}C_6Me_6)_2M]^{2+}$ cations, consistent with the observation of electrical conductivity.

Extended stacks of $(TCNQ)Me_2$ molecules with parallel stacks of $[(\eta^6\text{-}C_6Me_6)_2M]^{2+}$ cations are also present in the 1:3 phase **5a**, although the structure is not discussed in detail here due to the poor structural refinement (R = 0.17). This complex contains formally $[(TCNQ)Me_2]_3^{2-}$ entities in the stack, similar to those observed in $Cs_2(TCNQ)_3$.[35] Although the TCNQ molecules within the triad are crystallographically inequivalent, the poor refinement prohibits detailed discussion of bond lengths and angles and determination of the charge distribution within the $(TCNQ)Me_2$ stack. Therefore, one cannot distinguish crystallographically between electron delocalization along the entire anion stack or localization on $[(TCNQ)Me_2]_3^{2-}$ "supermolecules"[36] with

(35) Fritchie, C. J., Jr.; Arthur, P., Jr. *Acta Crystallogr.* **1966**, *21*, 139.
(36) Chestnut, D. B.; Arthur, P., Jr. *J. Chem. Phys.* **1962**, *36*, 2969.

Table XII. Atomic Positional Parameters for **4b**[a]

atom	x	y	z
Ru	0.0000	0.0000	0.0000
Cl1	0.2635 (3)	0.2636 (3)	0.3998 (2)
Cl2	0.8347 (2)	0.4526 (3)	0.4085 (2)
N18	0.935 (1)	0.231 (1)	0.6117 (8)
N19	0.544 (1)	0.072 (1)	0.7269 (9)
N28	0.5387 (9)	0.651 (1)	0.0838 (7)
N29	0.1659 (9)	0.468 (1)	0.1895 (8)
C1	0.1808 (8)	−0.0063 (8)	0.0852 (7)
C2	0.0518 (9)	0.0179 (9)	0.1813 (7)
C3	−0.0525 (8)	−0.0667 (8)	0.1974 (7)
C4	−0.0299 (9)	−0.1831 (8)	0.1191 (7)
C1	0.0014 (9)	−0.0832 (10)	0.1828 (10)
C6	0.2024 (8)	−0.1266 (9)	0.0087 (7)
C11	0.291 (1)	0.0378 (9)	0.0684 (9)
C12	0.027 (1)	0.141 (1)	0.2691 (9)
C13	−0.187 (1)	−0.039 (1)	0.2989 (9)
C14	−0.139 (1)	−0.278 (1)	0.1409 (9)
C15	0.125 (1)	−0.338 (1)	−0.0564 (9)
C16	0.342 (1)	−0.159 (1)	−0.090 (1)
C18	0.824 (1)	0.235 (1)	0.5934 (8)
C19	0.611 (1)	0.144 (1)	0.6625 (9)
C20	0.6878 (9)	0.2349 (9)	0.5815 (7)
C21	0.6200 (8)	0.3001 (8)	0.4937 (7)
C22	0.493 (1)	0.2643 (9)	0.4807 (7)
C23	0.4163 (9)	0.3226 (9)	0.4018 (7)
C24	0.4719 (8)	0.4268 (8)	0.3225 (6)
C25	0.5991 (9)	0.4602 (9)	0.3337 (6)
C26	0.6764 (9)	0.3995 (8)	0.4127 (7)
C27	0.4011 (9)	0.4951 (9)	0.2360 (7)
C28	0.4771 (9)	0.582 (1)	0.1527 (7)
C29	0.271 (1)	0.478 (1)	0.2158 (8)
H11A	0.259	0.157	0.126
H11B	0.377	0.030	0.082
H11C	0.310	0.115	−0.015
H12A	−0.064	0.143	0.328
H12B	0.102	0.134	0.312
H12C	0.027	0.223	0.222
H13A	−0.247	−0.109	0.296
H13B	−0.164	−0.042	0.378
H13C	−0.237	0.048	0.288
H14A	−0.109	−0.352	0.081
H14B	−0.150	−0.315	0.223
H14C	−0.229	−0.231	0.134
H15A	0.215	−0.343	−0.116
H15B	0.124	−0.416	−0.004
H15C	0.049	−0.335	−0.098
H16A	0.402	−0.089	−0.087
H16B	0.391	−0.245	−0.074
H16C	0.324	−0.160	−0.170
H22	0.454	0.193	0.533
H25	0.638	0.532	0.282

[a] Estimated standard deviations in the least significant digits are shown in parentheses.

geometrically inequivalent $(TCNQ)Me_2$ sites.

Discussion

Electrocrystallization. The single-crystal X-ray results and the trends observed in the synthesis of these charge-transfer complexes strongly suggest that a plausible source of the potential control of stoichiometry is the different relative concentrations of TCNQ and $TCNQ^-$ at the electrode during crystallization at different potentials, as described by the Nernst equation. It is reasonable to suggest that prenucleation aggregates that structurally resemble the macroscopic crystals are required for crystallization of a particular phase.[37] The single-crystal X-ray results, which indicate the presence of dimer dianions, imply that $[TCNQ]_2^{2-}$ may precede crystallization of the 1:2 phase, whereas a partially reduced TCNQ aggregate such as $[TCNQ]_2^-$ or $[TCNQ]_4^{2-}$ may initiate formation of the 1:4 phase, which *formally* contains equivalent amounts of $TCNQ^0$ and $TCNQ^-$ (Scheme I). When $E \geq E^\circ$ (i.e. very positive potentials), conditions are more favorable for the formation of partially reduced aggregates, and ultimately the 1:4 phase, since at the electrode [TCNQ] is more likely to be equal to or greater than $[TCNQ^-]$ under this condition. Conversely, at very negative potentials the predominant species at the electrode is $TCNQ^-$, favoring the presence of the fully reduced dimer dianion. The potential dependence of the $TCNQ/TCNQ^-$ ratio was confirmed by infrared optically transparent thin-layer electrochemistry. At open circuit and at positive potentials (vs a Ag-wire pseudoreference) a nitromethane solution of TCNQ exhibited a ν_{CN} absorption at 2222 cm^{-1}. As the potential was made more negative, the intensity of this band decreased with the concomitant appearance and increase of an absorption at 2180 cm^{-1} due to the $TCNQ^-$ anion. Interestingly, a small feature at 2200 cm^{-1} appeared when $TCNQ^-$ was generated, suggesting the presence of a $[TCNQ]_n^{(n/2)-}$ aggregate if a linear dependence of ν_{CN} on the extent of reduction is assumed.[16,17]

Although the existence of $[TCNQ]_2^{2-}$ has been reported in aqueous solvents, its concentration is not significant in nonaqueous solvents.[38] Presumably, Coulombic repulsion between the anions inhibits the formation of $[TCNQ]_2^{2-}$ in organic solvents but is alleviated by solvation effects in aqueous media. This suggests favorable crystallization kinetics for the formation of **1**. Additionally, the observation of potential-dependent control of stoichiometry strongly suggested that the crystallization rates of **1** and **2** at their respective growth potentials were not appreciably different.

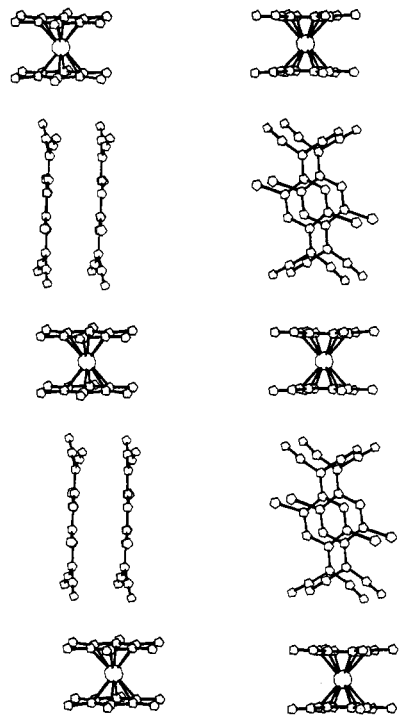

Figure 9. Illustrations of a single 1-D mixed ...DAADAA... stack in **4a** viewed parallel and perpendicular to the planes of the $[(TCNQ)Cl_2]_2^{2-}$ dimer dianion. Hydrogen atoms have been omitted for clarity.

Scheme I

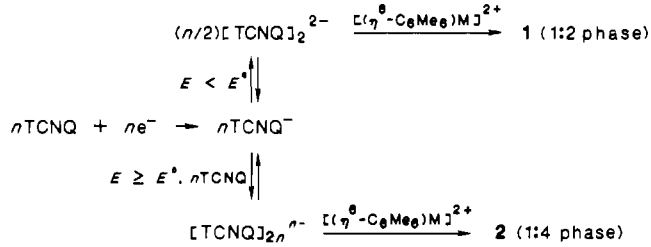

(37) Addadi, L.; Berkovitch-Yellin, Z.; Weissbuch, I.; van Mil, J.; Shimon, L. J. W.; Lahav, M.; Leiserowitz, L. *Angew. Chem., Int. Ed. Engl.* **1985**, *24*, 466.

(38) Boyd, R. H.; Phillips, W. D. *J. Chem. Phys.* **1965**, *43*, 2927.

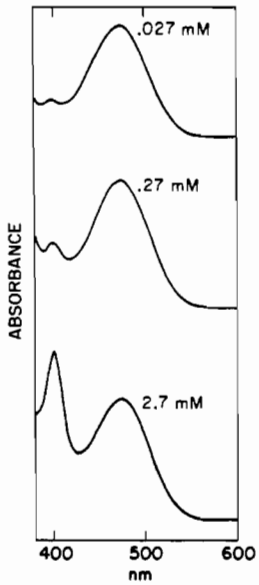

Figure 10. Concentration dependence of UV–visible spectra of $(TCNQ)Cl_2^-$ solutions in acetonitrile. The higher energy band is due to the dimer, and the lower energy absorption is attributed to the monomer.

The observation of different stoichiometry in these two phases clarifies a recent report that an unsatisfactory elemental analysis was obtained in the attempted synthesis of $[(\eta^6\text{-}C_6Me_6)_2Fe]^+[TCNQ]^-$ from the reaction of the 20-electron species $[(\eta^6\text{-}C_6Me_6)_2Fe]^0$ and TCNQ.[39] Since reduction of TCNQ or $TCNQ^-$ by the 19-electron $[(\eta^6\text{-}C_6Me_6)_2Fe]^+$ is thermodynamically favored ($E°(TCNQ^-/TCNQ^{2-}) = -0.35$ V vs SCE), it seems reasonable that $[(\eta^6\text{-}C_6Me_6)_2Fe]^{2+}$ was generated in the presence of TCNQ and $TCNQ^-$, resulting in the formation of a mixture of **1** and **2**. We have not observed any evidence for the formation of $[(\eta^6\text{-}C_6Me_6)_2Fe]^+[TCNQ]^-$, and its presence is not expected given the known redox behavior. Furthermore, the instability of bis(arene)transition metal complexes[40] in the presence of $TCNQ^{2-}$ may contribute to product impurity. The electrochemical methods described above using the dications are therefore more suitable for the preparation of these phases since formation of unstable organometallic intermediates and more highly reduced TCNQ anions is obviated.

The selectivity pattern observed with substituted TCNQ species are consistent with Scheme I. In contrast to the case for the $[TCNQ]_2^{2-}$ dimer, UV–vis spectroscopy revealed the presence of $[(TCNQ)Cl_2]_2^{2-}$ and $[(TCNQ)F_4]_2^{2-}$ in acetonitrile under conditions in which $[TCNQ]_2^{2-}$ was absent. The $[TCNQ]_2^{2-}$ dimer exhibits absorptions in water at 365 and 643 nm, whereas the monomer exhibits absorption bands at 409 and 737 nm. The equilibrium between the halogenated monomer and dimer anions in acetonitrile can be conveniently followed by the analogous absorptions, particularly the higher energy bands. At low concentrations the $(TCNQ)Cl_2^-$ anion exhibits a pronounced absorption at 476 nm, which decreased at higher concentrations with concomitant increase in the absorption at 404 nm attributed to the dimer dianion (Figure 10). In the case of $(TCNQ)F_4^-$, only the dimer absorption exists under these conditions. These results clearly demonstrate that the dimer dianion is more favored in solution when electron-withdrawing substituents are present. This appears to be made manifest in the exclusive formation of the 1:2 phase for $(TCNQ)F_4^-$ and $(TCNQ)Cl_2^-$, with dimer dianion entities in the solid state. We note that, to our knowledge, there are no examples of complex salts (i.e. fractional charge, $\rho < 1$) with $(TCNQ)F_4$, as the anions are always fully reduced and generally are dimerized. This further indicates that halogenated dimer dianions are rather stable, in solution as well as the solid state. Indeed, the intradimer separations decrease in the order TCNQ > $(TCNQ)Cl_2^-$ > $(TCNQ)F_4^-$. The apparent larger association constant and smaller interplanar separations for halogenated anions is consistent with lessened repulsion or possibly greater London dispersion forces when electronegative substituents are present. The observation that TCNQ anions with electron-donating groups prefer to form conducting phases which formally possess TCNQ anions with $\rho < 1$ may reflect the absence of the dimer dianions in solution necessary for formation of analogous 1:2 phases due to more significant Coulombic repulsion between anions. These repulsive interactions may be ameliorated by the dispersal of charge over a larger number of molecules through the formation of partially reduced aggregates, either in solution, in the nucleation events leading to crystallization, or in the solid state.

In addition to being a convenient route to these complexes that obviates unstable lower valent reagents, electrocrystallization allows more precise control of the crystallization process. Until recently, simultaneous growth of different phases during electrocrystallization of one-dimensional materials has not been extensively considered.[41] For example, electrocrystallization of superconducting bis(ethylenedithio)tetrathiafulvalene salts has been reported to occur with the formation of several different morphologies, which are presumably different phases.[42–44] The potential-dependent selectivity toward **1** and **2**, which is identical with observations we have recently made in the synthesis of $[(\eta^5\text{-}C_5Me_5)Ru([2.2](4,4)\text{-cyc})Ru(\eta^5\text{-}C_5Me_5)][TCNQ]_x$ ($x = 2, 4$)[45] ([2.2](4,4)cyc = [2.2](4,4)cyclophane) and $[(\eta^5\text{-}C_5Me_5)_2Fe][TCNQ]_x$ ($x = 1, 2$),[13] clearly demonstrates that the experimentally controllable parameters (i.e. potential and current) exert a pronounced effect on crystal growth and can be exploited to direct selectivity toward desired phases.

Furthermore, electrocrystallization can be used to prepare poorly conducting charge-transfer complexes as well as conducting phases, which are more commonly prepared by this method. Although electrochemical growth of insulating materials would be expected to result in the formation of resistive films that passivate the electrode, we have shown previously that the poorly conducting charge-transfer solid $[(\eta^5\text{-}C_5Me_5)_2Fe][TCNQ]$ could be prepared by this method; the well-formed crystalline habit of this complex allowed transport of solution to the electrode so that crystal growth could occur. Similarly, the 1:2 phases grew as fairly large crystals (ca. 1 mm^2) on only a very small portion of the electrode, favoring efficient mass transfer of solute to the electrode and obviating passivation of the electrode. Since these complexes are poorly conducting, this implies that crystal growth must occur at or very near the electrode–crystal interface.

Structural Aspects. The face-to-face stacking of the organometallic dications and the $[TCNQ]_2^{2-}$ dimer observed in **1a,b** resembles that commonly observed in organic DA solids,[12] and a DAAD segment of the linear chain is structurally similar to the motif reported for $[(\eta^5\text{-}C_5Me_5)_2Fe]_2[TCNQ]_2$.[2] However, to our knowledge, the stacking motif observed in the linear chains in **3** and **4** in which the planes of the anions are nearly perpendicular to those of the cation ligands has not been observed previously. The close proximity of the nitrogen atoms to the C_6Me_6 ligands observed in the 1:2 phases with halogenated TCNQ anions is significantly less than the sum of the van der Waals radii,[46] suggesting donor–acceptor interactions between these groups.[47]

(39) Desbois, M. H.; Michaud, P.; Astruc, D. *J. Chem. Soc., Chem. Commun.* **1985**, 450.
(40) Seidle, A. R.; Candela, G. A.; Finnegan, T. F. *Inorg. Chim. Acta* **1979**, *35*, 125.
(41) Williams, J. M.; Carneiro, K. *Adv. Inorg. Chem. Radiochem.* **1985**, *29*, 249.
(42) Parkin, S. S.; Engler, E. M.; Schumaker, R. R.; Lagier, R.; Lee, V. Y.; Scott, J. C.; Greene, R. L. *Phys. Rev. Lett.* **1983**, *50*, 270.
(43) Satio, G.; Enoki, T.; Toriumi, T.; Inokuchi, H. *Solid State Commun.* **1982**, *42*, 557.
(44) Williams, J. M.; Emge, T. J.; Wang, H. H.; Beno, M. A.; Copps, P. T.; Hall, L. N.; Carlson, K. D.; Crabtree, G. W. *Inorg. Chem.* **1984**, *23*, 2558.
(45) Ward, M. D.; Fagan, P. J.; Calabrese, J. C., to be submitted for publication.
(46) Bondi, A. *J. Phys. Chem.* **1964**, *68*, 441.
(47) Soos, Z. G. *Annu. Rev. Phys. Chem.* **1974**, *25*, 121.

In this regard, it is interesting to note that similar intermolecular contacts between a nitrogen atom of a $[(TCNQ)F_4]_2^{2-}$ dimer and a ring carbon of the neutral $(TCNQ)F_4$ molecule in $[(\eta^5\text{-}C_5H_5)_2Fe]_2[(TCNQ)F_4]_3$ have recently been reported.[48] We have previously reported that these dications exhibit a face-to-face arrangement with the planar $[C_6(CN)_6]^{2-}$ dianion to give the highly colored mixed-stack charge-transfer solids $[(\eta^6\text{-arene})_2M][C_6(CN)_6]$ (M = Fe, Ru).[11] However, **3** and **4** exhibit molecular interactions similar to those we have recently observed in $[(\eta^6\text{-arene})_2M][i\text{-}C_4(CN)_6]$ (M = Fe, Ru), which exhibits strong charge-transfer absorption bands in the visible spectrum as a result of short (<3.0 Å) contacts between the nitrogen atoms of the nonplanar dianion and the arene ligands of the dication.[49] We have not been able to distinguish the presence of charge-transfer bands resulting from these interactions in **3** and **4**, as the absorption spectra are dominated by the intense charge-transfer absorptions typical of the dimer dianions. Similar types of intermolecular contacts have been reported in $(\eta^6\text{-}C_6H_6)Cr(CO)_3$[50] and the charge-transfer complexes $[(\eta^6\text{-}C_6H_5OMe)Cr(CO)_3][C_6H_3(NO_2)_3]$[51] and $[(\eta^6\text{-pha})Cr(CO)_3][C_6H_3(NO_2)_3]$[52] (pha = phenanthrene). The former exhibited short contact distances between the carbonyl oxygen atoms and benzene ligand carbon atoms of another $(\eta^6\text{-}C_6H_6)Cr(CO)_3$ molecule, whereas the latter pair displayed charge-transfer behavior resulting from close approach of the carbonyl oxygen atoms and the trinitrobenzene molecule. Similarly, $[N,N\text{-}Me_2bpym][i\text{-}C_4(CN)_6]$ (N,N-Me_2bpym = N,N-dimethylbipyridinium) has been reported[53] to possess mixed stacks of cations and anions with short intermolecular contacts between the anion nitrogen atoms and the ring carbons of the cation (although these distances are not as short as those in **3** and **4**).

It is tempting to attribute the short intermolecular distances to σ interactions of the cyano nitrogen atoms with a low-lying ligand π^* orbital on the cation. Previous reports cite the presence of low-lying ligand orbitals in $[(\eta^6\text{-arene})_2M]^{2+}$ as the unoccupied metal e_{1g}^* (d_{xz},d_{yz}) and ligand e_{2u}^* (p_z) orbitals may be very close in energy,[54,55] resulting in extensive mixing of e_{2u}^* into the metal orbitals.[56,57] The exact orbital ordering is difficult to establish as it is very sensitive to charge as well as substitution on the arene rings, as shown by the systematic cathodic shift in reduction potential as methyl group substitution increases.[58] However, it has been reported that the lowest unoccupied molecular orbital in these cations may possess primarily ligand character.[59] The observation that the C_6H_6 ring of $[(\eta^6\text{-}C_6H_6)Ru(\eta^6\text{-}C_6Me_3H_3)]^{2+}$ is readily attacked by hydride[60] is also consistent with the presence of a low-lying ligand orbital. We have also performed extended Hückel calculations, which indicate low-lying orbitals localized on the hexamethylbenzene ligands.

The reasons for the markedly different solid-state structures of the 1:2 phases are not yet well-understood. Although the short intermolecular contacts in **3** and **4** suggest charge-transfer interactions between the cyano nitrogen atoms and the arene ligands that may influence the structural motif, the solid-state structure may be more strongly influenced by charge distributions within the dimer dianions, which may play a role in Madelung lattice energies. It is readily obvious that the unit cells of **1**, **3**, and **4** (Figure 1) are essentially identical except for the orientation of the dimer dianion and that the molecular packing results in favorable electrostatic interactions between the cations and dimer dianions. It is to be expected that the charge distribution in the halogenated dimer dianions would differ significantly from that in $[TCNQ]_2^{2-}$ as the halogenated anions would tend to inductively withdraw charge toward the electronegative substituents compared to TCNQ, which possesses excess negative charge on the exocyclic methylidene carbon.[15] Translation along the c axis in **3** and the b axis in **4** shows the cation alongside the rings of the dimer dianions, suggesting Coulombic attractive forces may be an important factor in the observed orientation. In the case of **1a,b** the dication resides in proximity to the exocyclic $C(CN)_2$ moiety when viewed by translation along the a and b axes.

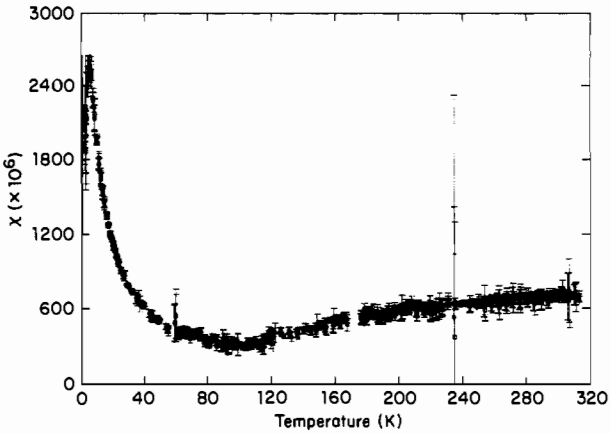

Figure 11. Temperature-dependent magnetic susceptibility data for **2a**.

Electronic Properties. The mixed-stack 1:2 phases exhibited room-temperature conductivities $<10^{-7}\ \Omega^{-1}\ cm^{-1}$. The low conductivities are consistent with the single-crystal X-ray results, which revealed a mixed stack of donors and acceptors with little evidence of extended interaction between $TCNQ^-$ anions. The measured magnetic susceptibilities of the nonconducting 1:2 phases were diamagnetic and temperature-independent over the entire temperature range investigated (2–325 K) and are also consistent with the structural results, which indicate pairing of $TCNQ^-$ anions. The value of the diamagnetic susceptibilities generally agreed with the results expected from Pascal's constants.[61] Closer correspondence was realized when diamagnetic corrections of the molecular constituents were obtained from susceptibility measurements of simple salts of the cations and anions. The results indicate that the 1:2 phases can be considered as simple ionic solids, with negligible donor–acceptor interactions.

The electrical conductivities of the 1:4 phases **2a,b** were much higher than those observed for the 1:2 phases, suggesting extended interactions among TCNQ arrays implied by preliminary structural results. The temperature dependence of the conductivity of these phases, measured by using compacted-powder samples due to the poor crystalline quality of the material, indicated semiconducting behavior (i.e. positive temperature coefficient) with an activation energy E_a = 0.06 eV.[62]

The lack of structural data and the use of compacted-powder samples complicate definitive interpretation of the electronic behavior. However, a plausible explanation for the observations is electronic localization along the TCNQ stack due to Coulomb repulsion energies that are larger than the bandwidth.[63] In

(48) Miller, J. S.; Zhang, J. H.; Reiff, W. M. *Inorg. Chem.* **1987**, *26*, 600.
(49) Ward, M. D.; Farlee, R. D., submitted for publication.
(50) (a) Bailey, M. F.; Dahl, L. F. *Inorg. Chem.* **1965**, *4*, 1314. (b) Rees, B.; Coppens, P. *Acta Crystallogr., Sect. B: Struct. Crystallogr. Cryst. Chem.* **1973**, *B29*, 2515.
(51) (a) Carter, L.; McPhail, A. T.; Sim, G. A. *J. Chem. Soc. A* **1966**, 822. (b) Kobayashi, H.; Kobayashi, K.; Kaizu, Y. *Inorg. Chem.* **1981**, *20*, 4135.
(52) De, R. L.; Von Seyerl, J.; Zsolnai, L.; Huttner, G. *J. Organomet. Chem.* **1979**, *175*, 185.
(53) Nakamura, K.; Kai, Y.; Yasuoka, N.; Kasai, N. *Bull. Chem. Soc. Jpn.* **1981**, *54*, 3300.
(54) Anderson, S. E., Jr.; Drago, R. S. *Inorg. Chem.* **1972**, *11*, 1564.
(55) Brintzinger, H.; Palmer, G.; Sands, R. H. *J. Am. Chem. Soc.* **1965**, *87*, 623.
(56) Morrison, W. H.; Ho, E. Y.; Hendrickson, D. N. *Inorg. Chem.* **1975**, *14*, 500.
(57) Anderson, S. E., Jr.; Drago, R. S. *J. Am. Chem. Soc.* **1970**, *92*, 4244.
(58) Hamon, J. R.; Astruc, D.; Michaud, P. *J. Am. Chem. Soc.* **1981**, *103*, 758.
(59) Clack, D. W.; Warren, K. D. *J. Organomet. Chem.* **1978**, *152*, C60.
(60) Rybinskaya, M. I.; Kaganovich, V. S.; Kudinov, A. R. *J. Organomet. Chem.* **1982**, *235*, 215.
(61) Mula, L. N.; Boudreaux, E. A. *Theory and Applications of Molecular Diamagnetism*; Wiley-Interscience: New York, 1976.
(62) The activation energy was determined from the slope of log σ vs $1/T$, where $\sigma = \sigma_0 \exp(-E_a/kT)$.
(63) (a) Torrance, J. B. *Acc. Chem. Res.* **1979**, *12*, 79. (b) Garito, A. F.; Heeger, A. J. *Acc. Chem. Res.* **1973**, *7*, 232.

molecular terms, this localization may result in the formation of ...$(AA)^-(AA)^-(AA)^-(AA)^-$... sites. Within this assumption, the observed activation energy is that needed for electronic transitions across an energy gap created by the Coulomb correlation, similar to the Mott transition energy invoked to explain the poor conductivity of simple TCNQ salts. The activation energy is that required to overcome Coulombic repulsion associated with formation of ...$(AA)^-(AA)^0(AA)^{2-}(AA)^-$... sites during charge transport. The relatively small activation energy observed for **2** is attributed to the larger size of the aggregate upon which localization occurs (i.e. one negative charge per two TCNQ molecules) compared to the size of simple salts, which substantially reduces the Coulomb repulsion energy.[64]

The susceptibilities for both the iron and the ruthenium 1:4 phases **2a,b** support the existence of extended acceptor–acceptor interactions. The susceptibilities of both compounds consisted of a small, low-temperature, Curie-like susceptibility and a weakly temperature dependent paramagnetic susceptibility superimposed upon the diamagnetic susceptibility resulting from the atomic core electrons. An example of the temperature-dependent susceptibility of the iron phase **2a** (with diamagnetic correction) is shown in Figure 11. Different samples qualitatively exhibited similar characteristics, although the relative size of the "Curie" component when compared to the higher temperature paramagnetism varied slightly from sample to sample, possibly due to variations in purity or defect concentration.

The susceptibility of **2a,b** is qualitatively similar to that observed for $(quin)(TCNQ)_2$ (quin = quinolinium), whose behavior has been interpreted according to the random exchange Heisenberg antiferromagnetic coupling (REHAC)[65,66] model. In this model the sites with the strongest coupling will be the first to spin pair, and as T is further lowered, pairing of spins with exchange coupling larger than kT will occur. In $(quin)(TCNQ)_2$, the randomness of the exchange coupling is thought to arise from disorder of the asymmetric cation, which induces localization of spins at low temperature with a random distribution of spacings, and therefore a random distribution of exchange coupling, between unpaired spins. Likewise a high degree of cation disorder, which prevented structural refinement of the X-ray data, was also observed in **2a,b**.

The REHAC model predicts a positive susceptibility at high temperatures, where kT is large compared to the exchange coupling, J, which is relatively independent of temperature similar to that predicted for a 1-D Heisenberg antiferromagnet.[67] As the temperature is lowered such that the average energy of a spin is below the average exchange coupling energy, the majority of the spins in the system will become antiferromagnetically aligned, resulting in a decrease in the observed susceptibility. The data in Figure 11 reflect this behavior as χ decreases gradually from 300 to 120 K. The susceptibility remains positive below 120 K due to uncoupled paramagnetic sites. The non-zero magnitude of χ is in accord with the 1-D Heisenberg antiferromagnetic model; however, $\chi_{min} = 0.52\chi_{max}$, which is slightly less than the value predicted for a 1-D Heisenberg antiferromagnet ($\chi_{min} = 0.69\chi_{max}$). The lower value of χ_{min} suggests some degree of 3-D antiferromagnetic ordering that is not accounted for by the Heisenberg model.

Below 80 K χ increases in a Curie-like manner. The REHAC model predicts a sub-Curie dependence ($C \propto T^{-b}$, where $b \cong 0.8$) in the susceptibility at low temperatures that results from paramagnetic sites; the sub-Curie dependence is due to random, weak exchange coupling between these sites. This behavior is observed for **2a,b** as the value of b obtained from the slope of log χ vs log T plots varied between 0.80 and 0.87. The variability in the susceptibility measurements suggests that the degree of antiferromagnetic exchange is very sensitive to sample preparation, owing to difficulty in controlling the spacing (and thus the exchange) between unpaired spins. An additional factor that affects the value of b is the number of paramagnetic impurities and defects in the sample. We also note that the presence of interspersed variable-length paramagnetic odd and diamagnetic even chain segments has also been proposed to account for this type of magnetic behavior in 1-D solids.[68] If this model is invoked, the relative amounts of even and odd chain segments in different samples may be responsible for the observed variability.

Concluding Remarks

These results demonstrate that the $[(\eta^6\text{-}C_6Me_6)_2M]^{2+}$ cations have the ability to form unique low-dimensional materials with appropriate acceptor anions. Indeed, the solid-state motif of mixed-stack linear chains containing halogenated TCNQ dimer dianions differs significantly from the face-to-face stacking commonly observed in 1-D solids. This suggests that unconventional modes of intermolecular interactions can be considered when designing new charge-transfer solids. The selectivity toward different phases can be substantially affected by the electrochemical parameters during crystal growth as well as the components that eventually comprise the charge-transfer solids. The electrochemically directed selectivity appears to be a general phenomenon, as we have recently observed identical behavior with $[(\eta^5\text{-}C_5Me_5)Ru([2.2](4,4)cyc)Ru(\eta^5\text{-}C_5Me_5)][TCNQ]_x$ (x = 2, 4)[45] and $[(\eta^5\text{-}C_5Me_5)_2Fe][TCNQ]_x$ (x = 1, 2).[13] Since the solid-state structure of a molecular solid ultimately determines its physical and electronic properties, the ability to rationally control the stoichiometry of charge-transfer complexes and to precisely regulate the crystal growth can have significant impact on this area.

Experimental Section

Materials. Acetonitrile was distilled from CaH_2 under nitrogen and nitromethane from $CaSO_4$ under nitrogen. Tetra-*n*-butylammonium tetrafluoroborate was recrystallized from ethyl acetate–ethanol and dried in vacuo prior to use. Literature methods were used for the preparation of $[(\eta^6\text{-}C_6Me_6)_2Fe][PF_6]_2$,[69] $[(\eta^6\text{-}C_6Me_6)_2Ru][BF_4]$,[70] and $[Bu_4N][TCNQ]$.[71] Derivatized TCNQ compounds, previously prepared by literature methods,[72] were obtained from R. C. Wheland (Du Pont).

Equipment. All manipulations were performed under inert-atmosphere conditions by using either purified nitrogen or a Vacuum Atmospheres glovebox. Electrocrystallizations were performed with a Princeton Applied Research 173 potentiostat using a Ag/AgCl reference electrode purchased from Bioanalytical Systems, Inc., in a standard H-cell with a fritted-glass separator. Platinum foils (0.5 × 0.5 cm) were used as the working and auxiliary electrodes. Infrared optically transparent thin-layer electrochemical experiments were performed with a Nicolet FT-IR spectrometer and an electrochemical cell constructed from two potassium bromide plates separated by a Teflon spacer. A platinum minigrid located in the center of the cell was employed as the working electrode, a platinum minigrid on the periphery of the cell as the counter electrode, and a silver wire as a pseudo reference electrode.

The magnetic susceptibility data was collected over the range 1.8–325 K by using a high-sensitivity computer-interfaced Faraday balance. Samples were suspended on a 1-mm quartz rod from the arm of a Cahn 2000 electrobalance. The sample container (4.2 × 10 mm) was fashioned from high-purity Spectrosil quartz. An electromagnet (Walker Scientific) supplied variable fields up to 22.5 kG. The magnetic field gradient was calibrated by using $HgCo(SCN)_4$ as a standard and varied by less than 1% in the area of the sample container. Temperature was controlled with a digital temperature controller (Oxford Instruments 3120) using a Au/Fe versus chromel-P thermocouple. A calibrated silicon diode resistance thermometer was used to measure the sample temperature, independently of the controlling thermocouple, over the entire temperature range. The Cahn balance was operated on the 100-mg scale, on which a sensitivity, under ideal conditions, of 0.001 mg can be achieved. Under normal operating conditions the sensitivity is the larger of 0.02

(64) Edwards, P. P.; Sienko, M. J. *Phys. Rev.* **1978**, *17*, 2575.
(65) Bulaevskii, L. N.; Zvarykina, A. V.; Karimov, Y. S.; Lyubovskii, R. B.; Shchegolev, I. F. *Zh. Eksp. Teor. Fiz.* **1972**, *35*, 725; *Sov. Phys.—JETP (Engl. Transl.)* **1972**, *35*, 384.
(66) Sanny, J.; Clark, W. G. *Solid State Commun.* **1980**, *35*, 473.
(67) Bonner, J. C.; Fisher, M. E. *Phys. Rev.* **1964**, *135*, 640.
(68) Soos, Z. G.; Bondeson, S. R. *Mol. Cryst. Liq. Cryst.* **1982**, *85*, 19.
(69) Helling, J. F.; Braitsch, D. M. *J. Am. Chem. Soc.* **1970**, *92*, 7207.
(70) Bennett, M. A.; Matheson, T. W. *J. Organomet. Chem.* **1979**, *175*, 87.
(71) Acker, D. S.; Harder, R. J.; Hertler, W. R.; Mahler, W.; Melby, L. R.; Benson, R. E.; Mochel, W. E. *J. Am. Chem. Soc.* **1960**, *82*, 6408.
(72) Wheland, R. C.; Martin, E. L. *J. Org. Chem.* **1975**, *40*, 3101.

Table XIII. Experimental Details for $[(\eta^6\text{-}C_6Me_6)_2Fe]^{2+}$–TCNQ Complexes

	$[(\eta^6\text{-}C_6Me_6)_2Fe][TCNQ]_2$ (**1a**)	$[(\eta^6\text{-}C_6Me_6)_2Fe][(TCNQ)F_4]_2$ (**3a**)	$[(\eta^6\text{-}C_6Me_6)_2Fe][(TCNQ)Cl_2]_2$ (**4a**)
mol formula	$C_{48}H_{44}N_8Fe$	$C_{49}H_{39}F_8N_9O_2Fe$	$C_{48}H_{40}N_8Cl_4Fe$
fw	788.79	933.75	926.21
cryst dimens, mm	0.10 × 0.20 × 0.25	0.10 × 0.20 × 0.40	0.30 × 0.03 × 0.05
peak width at half-height, deg	0.20	0.30	0.35
source	Mo Kα (λ = 0.71073 Å)	Mo Kα (λ = 0.71073 Å)	Mo Kα (λ = 0.71073 Å)
temp, °C	23 ± 1	23 ± 1	−92 ± 1
space group	$P\bar{1}$	$P\bar{1}$	$P\bar{1}$
a, Å	10.167 (2)	10.140 (3)	9.985 (6)
b, Å	11.281 (3)	10.907 (4)	11.116 (5)
c, Å	9.187 (1)	10.056 (4)	9.725 (7)
α, deg	111.08 (2)	95.74 (3)	104.28 (7)
β, deg	98.10 (1)	93.72 (3)	98.07 (5)
γ, deg	92.37 (2)	92.35 (3)	89.88 (6)
V, Å^3	968.5	1103.0	1035 (2)
d, g cm^{-3}	1.35	1.50	1.49
μ, cm^{-1}	4.5	4.5	6.81
soln	Patterson method	Patterson method	direct methods
H atoms	located and refined isotropically	not included	included in calcd positions (d_{C-H} = 0.95 Å)
no. of reflns included	1900 with $F_o^2 > 3.0\sigma(F_o^2)$	1573 with $F_o^2 > 3.0\sigma(F_o^2)$	1304 with $F_o^2 > 2.58\sigma(F_o^2)$
no. of parameters refined	350	322	277
unweighted agreement factor	0.046	0.068	0.078
weighted agreement factor	0.052	0.082	0.097
esd of observn of unit wt	1.25	1.97	1.68
convergence, largest shift	0.22σ	0.04σ	0.01σ
high peak in final diff map, e Å^{-3}	0.29 (5)	0.59 (8)	1.57
scan type	ω–θ	ω–θ	ω–2θ
scan rate in ω, deg min^{-1}	2–20	2–20	2–20
scan width, deg	0.7 + 0.350 tan θ	1.0 + 0.350 tan θ	1.0 + 0.35 tan θ
max, 2θ, deg	50.0	50.0	50.0
no. of reflns measd	3517 total, 3387 unique	4032 total, 3860 unique	3629 total
cor	Lorentz–polarizn, linear decay (from 1.00 to 1.03 on I)	Lorentz–polarizn, linear decay (from 0.97 to 1.11 on I), empirical abs (from 0.79 to 1 on I)	Lorentz–polarizn

mg or 0.1% of the force being measured. A typical error estimate in the measurement of the susceptibilities reported in this paper is 0.5%. The susceptibilities have been corrected for the intrinsic diamagnetism of the sample container and the diamagnetism of the electronic cores of the constituent atoms.

Spectroscopic Measurements. Infrared spectra were recorded on a Nicolet 7199 Fourier transform spectrometer.

Synthesis of $[(\eta^6\text{-}C_6Me_6)_2Fe][TCNQ]_2$ (1a). Analytically pure **1a** was prepared as a microcrystalline solid by slow addition of $[Bu_4N][TCNQ]$ (90 mg, 0.2 mmol) in 10 mL of acetonitrile to $[(\eta^6\text{-}C_6Me_6)_2Fe][PF_6]_2$ (67 mg, 0.1 mmol) in 10 mL of acetonitrile. The precipitate was washed three times with 5 mL of acetonitrile and dried in vacuo to yield deep purple product in quantitative yield. Single crystals could be grown in small amounts from acetonitrile by slow diffusion methods.

Electrocrystallization of 1a. A standard H-cell with a glass fine-porosity separator containing a nitromethane solution of 0.1 M Bu_4NBF_4 in both chambers was prepared. To the working compartment was added $[(\eta^6\text{-}C_6Me_6)_2Fe][PF_6]_2$ (50 mg, 0.075 mmol) and TCNQ (31 mg, 0.15 mmol) and the cell sealed with platinum electrodes in both sides and an Ag/AgCl reference in the working side. The cell was biased at −0.1 V (vs SCE), upon which purple X-ray-quality crystals of **1** rapidly formed on the electrode. After 1.45 C had passed through the cell (10% conversion), the crystals were harvested by filtration and washed three times with nitromethane. The formation of **1** was occasionally accompanied by small amounts of $[(\eta^6\text{-}C_6Me_6)_2Fe][TCNQ]_4$ (**2a**) (see below).

Electrocrystallization of 1b. The ruthenium analogue $[(\eta^6\text{-}C_6Me_6)_2Ru][TCNQ]_2$ (**1b**) was prepared by identical methods from $[(\eta^6\text{-}C_6Me_6)_2Ru][BF_4]_2$ (45 mg, 0.075 mmol) and TCNQ (31 mg, 0.15 mmol), but **1b** was the only product at the electrode and was not contaminated by $[(\eta^6\text{-}C_6Me_6)_2Ru][TCNQ]_4$ (**2b**). Filtration of the working compartment solution after 1.45 C had passed through the cell (10% conversion) gave **1b** as high-quality purple crystals (6.0 mg, Faradaic yield 95%).

Electrocrystallization of $[(\eta^6\text{-}C_6Me_6)_2Fe][TCNQ]_4\cdot 2CH_3NO_2$ (2a). A standard H-cell with a glass fine-porosity separator containing a nitromethane solution of 0.1 M Bu_4NBF_4 in both chambers was prepared. To the working compartment was added $[(\eta^6\text{-}C_6Me_6)_2Fe][PF_6]_2$ (50 mg, 0.075 mmol) and TCNQ (31 mg, 0.15 mmol) and the cell sealed with platinum electrodes in both sides and an Ag/AgCl reference in the working side. The cell was biased at +0.4 V (vs SCE) and left to stand for several days. Black needle-shaped crystals slowly grew at the electrode surface. After 1.45 C had passed through the cell (10% conversion), the product was harvested by filtration and washed three times with nitromethane to yield black crystals of **2a** (9.1 mg, Faradaic yield 92%).

Electrocrystallization of 2b. The ruthenium analogue $[(\eta^6\text{-}C_6Me_6)_2Ru][TCNQ]_4\cdot 2CH_3NO_2$ (**2b**) was prepared by identical methods from $[(\eta^6\text{-}C_6Me_6)_2Ru][BF_4]_2$ (45 mg, 0.075 mmol) and TCNQ (31 mg, 0.15 mmol). After 1.45 C had passed through the cell (10% conversion), the product was harvested by filtration and washed three times with nitromethane to yield black crystals of **2b** (9.8 mg, Faradaic yield 96%).

Electrocrystallization of $[(\eta^6\text{-}C_6Me_6)_2Fe][(TCNQ)F_4]_2$ (3a). A standard H-cell with a glass fine-porosity separator containing a nitromethane solution of 0.1 M Bu_4NBF_4 in both chambers was prepared. To the working compartment was added $[(\eta^6\text{-}C_6Me_6)_2Fe][PF_6]_2$ (50 mg, 0.075 mmol) and $(TCNQ)F_4$ (41 mg, 0.15 mmol) and the cell sealed with platinum electrodes in both sides and an Ag/AgCl reference in the working side. The cell was biased at +0.4 V (vs SCE) and left to stand for several days. Purple crystals of **3a** grew slowly at the electrode surface. After 1.45 C had passed through the cell (10% conversion), the product was harvested by filtration and washed three times with nitromethane (7.0 mg, Faradaic yield 100%). The ruthenium analogue **3b** was prepared by identical methods using $[(\eta^6\text{-}C_6Me_6)_2Ru][BF_4]_2$.

Electrocrystallization of $[(\eta^6\text{-}C_6Me_6)_2Fe][(TCNQ)Cl_2]_2$ (4a). A standard H-cell with a glass fine-porosity separator containing a nitromethane solution of 0.1 M Bu_4NBF_4 in both chambers was prepared. To the working compartment was added $[(\eta^6\text{-}C_6Me_6)_2Fe][PF_6]_2$ (50 mg, 0.075 mmol) and $(TCNQ)Cl_2$ (41 mg, 0.15 mmol) and the cell sealed with platinum electrodes in both sides and an Ag/AgCl reference in the working side. The cell was biased at +0.33 V (vs SCE) and left to stand for several days. Purple crystals of **4a** grew slowly at the electrode surface. After 1.45 C had passed through the cell (10% conversion), the product was harvested by filtration and washed three times with nitromethane (6.5 mg, Faradaic yield 95%). The ruthenium analogue **4b** was prepared by identical methods with $[(\eta^6\text{-}C_6Me_6)_2Ru][BF_4]_2$.

X-ray Data Collection and Data Reduction.[73] Preliminary examination and data collection were performed on an Enraf-Nonius CAD4 computer-controlled κ-axis diffractometer equipped with a graphite crystal, incident beam monochromator. Tables XIII and XIV summarize

(73) These services were performed by either the Molecular Structure Corp. (**1a**, **3a**, **4a**) or the Oneida Research Corp. (**1b**, **3b**, **4b**).

Table XIV. Experimental Details for $[(\eta^6\text{-}C_6Me_6)_2Ru]^{2+}$–TCNQ Complexes

	$[(\eta^6\text{-}C_6Me_6)_2Ru][TCNQ]_2$ (**1b**)	$[(\eta^6\text{-}C_6Me_6)_2Ru][(TCNQ)F_4]_2$ (**3b**)	$[(\eta^6\text{-}C_6Me_6)_2Ru][(TCNQ)Cl_2]_2$ (**4b**)
mol formula	$C_{48}H_{44}N_8Ru$	$C_{49}H_{39}F_8N_9O_2Ru$	$C_{48}H_{40}Cl_4N_8Ru$
fw	834.01	1038.97	900.88
cryst dimens, mm	0.10 × 0.30 × 0.32	0.24 × 0.28 × 0.32	0.15 × 0.24 × 0.38
peak width at half-height, deg	0.48	0.59	0.71
source	Cu Kα (λ = 1.541 84 Å)	Cu Kα (λ = 1.541 84 Å)	Mo Kα (λ = 0.710 73 Å)
temp, °C	−35 (1)	−35 (1)	23 (1)
space group	$P\bar{1}$	$P\bar{1}$	$P\bar{1}$
a, Å	11.350 (7)	10.143 (8)	9.993 (11)
b, Å	9.163 (3)	10.830 (2)	11.225 (10)
c, Å	10.184 (5)	10.092 (5)	9.838 (6)
α, deg	91.82 (5)	92.11 (4)	89.21 (8)
β, deg	110.89 (4)	96.40 (3)	75.36 (7)
γ, deg	98.19 (3)	94.40 (5)	81.98 (7)
V, Å^3	976 (2)	1097 (2)	1057 (2)
d, g cm^{-3}	1.42	1.57	1.42
μ, cm^{-1}	36.6	37.0	5.3
soln	Patterson method	Patterson method	Patterson method
H atoms	refined with B_{iso} = 5.0 Å^2	included as fixed contribn to the structure factor	included as fixed contribn to the structure factor
no. of reflns included	2822 with $F_o^2 > 2.0\sigma(F_o^2)$	3098 with $F_o > 2.0\sigma(F_o^2)$	2386 with $F_o^2 > 3.0\sigma(F_o^2)$
no. of params refined	328	310	280
unweighted agreement factor	0.039	0.065	0.069
weighted agreement factor	0.043	0.073	0.075
esd of observn of unit wt	1.10	1.91	1.98
convergence, largest shift	0.58σ	0.21σ	0.00σ
high peak in final diff map, e Å^{-3}	1.52 (7)	1.01 (12)	1.40 (11)
scan type	ω–θ	ω–θ	ω–θ
scan rate in ω, deg min^{-1}	3–5	3–5	3–5
scan width, deg	1.2 + 0.140 tan θ	1.4 + 0.140 tan θ	1.5 + 0.140 tan θ
no. of reflns measd	2901 total, 2863 unique	3267 total, 3174 unique	2906 total, 2829 unique
cor	Lorentz–polarizn, linear decay (from 0.938 to 1.029 on I)	Lorentz–polarizn, linear decay (from 1.001 to 1.349 on I)	Lorentz–polarizn, linear decay (from 0.926 to 1.063 on I), empirical abs (from 0.59 to 1.00 on I)

the relevant conditions of data collection.

Cell constants and an orientation matrix for data collection were obtained from least-squares refinement, measured by the computer-controlled diagonal slit method of centering. The number of setting angles and the range are given in the supplementary material.

As a check on crystal and electronic stability three representative reflections were measured every 41 min (for the iron series) or 30 min (for the ruthenium series). The intensities of these standards changed for all the complexes with the exception of $[(\eta^6\text{-}C_6Me_6)_2Ru][(TCNQ)\text{-}Cl_2]_2$. A linear decay correction was applied for the iron series and an anisotropic decay correction for the ruthenium series (see the supplementary material).

Structure Solution and Refinement. Relevant conditions are summarized in Tables XIII and XIV. The structures were solved by either direct or Patterson methods. Hydrogen atoms were located, and if possible, their positions and isotropic thermal parameters were refined. The structures were refined in full-matrix least squares where the function minimized was $\sum w(|F_o| - |F_c|)^2$ and the weight w is defined as $4F_o^2/s^2(F_o^2)$. The standard deviation on intensities, $s^2(F_o^2) = [S^2(C + R^2B) + (PF_o^2)^2]/Lp^2$ where S is the scan rate, C is the total integrated peak count, R is the ratio of scan time to background counting time, B is the total background count, Lp is the Lorentz–polarization factor, and the parameter P (ignorance factor) is a factor introduced to downweight intense reflections.

Scattering factors were taken from Cromer and Waber.[74] Anomalous dispersion effects were included in F_c;[75] the values for $\Delta f'$ and $\Delta f''$ were those of Cromer.[76] Only the reflections having intensities greater than 3.0 times their standard deviation were used in the refinements. The final cycle of refinement converged with unweighted and weighted agreement factors according to

$$R_1 = \sum||F_o| - |F_c||/\sum|F_o| \qquad R_2 = (\sum w(|F_o| - |F_c|)^2/\sum wF_o^2)^{1/2}$$

The heights of the highest peaks in the final different Fouriers are given in Tables XIII and XIV. Plots of $\sum w(|F_o| - |F_c|)^2$ versus $|F_o|$, reflection order in data collection, sin (q/l), and various classes of indices showed no unusual trends for any of the compounds.

Acknowledgment. We thank E. J. Delawski and R. S. McLean (Du Pont) for technical assistance and A. Epstein (The Ohio State University) for helpful discussions.

Registry No. **1a**, 71357-00-1; **1b**, 104531-37-5; **2a**, 104507-53-1; **2b**, 104531-38-6; **3a**, 111112-72-2; **3b**, 111112-74-4; **4a**, 111112-73-3; **4b**, 111112-75-5; **5a**, 111139-82-3; $[(\eta^6\text{-}C_6Me_6)_2Fe][TCNQ(OMe)_2]_x$, 111139-61-8.

Supplementary Material Available: Experimental details, tables of the thermal parameters, general temperature factors, bond distances, bond angles, torsion angles, intermolecular contacts, and weighted least-squares planes and figures with numbering schemes for **1a**,**b**, **3a**,**b**, and **4a**,**b** (157 pages); listings of structure factors for all compounds (73 pages). Ordering information is given on any current masthead page.

(74) Cromer, D. T.; Waber, J. T. *International Tables for X-Ray Crystallography*; Kynoch: Birmingham, England, 1974; Vol. IV, Table 2.2B.
(75) Ibers, J. A.; Hamilton, W. C. *Acta Crystallogr.* **1964**, *17*, 781.
(76) Cromer, D. J. *International Tables for X-Ray Crystallography*; Kynoch: Birmingham, England, 1974; Vol. IV, Table 2.3.1.